International Journal of Mechanical Sciences 263 (2024) 108771

Contents lists available at ScienceDirect

International Journal of Mechanical Sciences

journal homepage: www.elsevier.com/locate/ijmecsci

Generalized micromechanical formulation of fiber orientation tensor evolution equations

Tobias Karl [a,b,*], Thomas Böhlke [a]

[a] Institute of Engineering Mechanics, Chair for Continuum Mechanics, Karlsruhe Institute of Technology (KIT), Kaiserstraße 10, 76131 Karlsruhe, Germany
[b] Institute of Fluid Mechanics, Karlsruhe Institute of Technology (KIT), Kaiserstraße 10, 76131 Karlsruhe, Germany

ARTICLE INFO

Keywords:
Fiber orientation
Fiber suspensions
Homogenization
Anisotropy
Composites
Short fibers

ABSTRACT

Fiber orientation tensors are widely used to efficiently describe the fiber orientation evolution of anisotropic fiber suspensions during mold-filling. Real viscous fiber suspensions show fiber-induced anisotropic behavior. It is an open question how to correctly account for the anisotropic microstructure of fiber suspensions in general in the evolution equation of the fiber orientation tensors. In this study, a generalized evolution equation for the fiber orientation tensor of arbitrary even order is formulated, which takes into account the microstructural anisotropy of the fiber suspension. This formulation is based on a linear homogenization approach which allows the application of arbitrary mean-field models. The derived interaction term, representing the anisotropic environment of a single fiber, is discussed as a micromechanical convergence criterion of the underlying integral operator. It is shown and discussed in detail how the special cases of the Jeffery equation and the Folgar–Tucker equation follow from this general formulation. In addition, the generalized evolution equation is specified for selected mean-field models. In this context, an equation is presented to describe the evolution of the fiber orientation tensor depending on the spatial distribution of the fibers. For simple shear flow, all models describing the orientation dynamics are numerically investigated and compared. The results for the second-order orientation tensor as well as for a single fiber show that the well-known periodic behavior is present and strongly depends on the volume fraction and the chosen mean-field model. Considering the spatial distribution of the fibers has a significant effect on the orientation evolution and strongly affects the periodic reorientation.

1. Introduction

Section content. The section at hand consists of an overview of the relevant state of the art and also describes the contributions to the field. In addition, the structure of the study is described and the tensor notation used is presented.

1.1. Motivation and state of the art

Predicting the evolution of fiber orientation during mold-filling is crucial for estimating the anisotropic properties of fiber suspensions and fiber reinforced composites [1]. As part of a simulative approach to lightweight design, models for a reliable orientation prediction are needed to implement a virtual process chain [2–4] in engineering practice. In this context, the original work of Jeffery [5,6] and more recent works incorporating narrow gaps, e.g., [7,8], inertia effects, e.g., [9–11], non-Newtonian fluids or second-order fluids, e.g., [12–14] or special particle geometries, e.g., [15,16] consider the orientation behavior of a single fiber. In contrast, the computationally efficient concept of orientation tensors [17,18] is widely used with the orientation evolution during mold-filling described by, e.g., the Folgar–Tucker equation [18,19], the reduced-strain closure model [20] or the anisotropic rotary diffusion model [21]. These equations are mostly formulated for second-order orientation tensors, and at most for fourth-order orientation tensors, with evolution equations for arbitrary higher order orientation tensors remaining an open topic. The mold-filling process itself can be modeled decoupled, i.e. the fiber-induced anisotropic viscosity is neglected. This stands in contrast to the coupled approach, where the fiber suspension is modeled with anisotropic viscosity, leading to an influence of the fiber orientation evolution on the flow field. Numerous studies investigate the effects of flow-fiber coupling, including early works, e.g., [22,23] and more recent works, e.g., [24–27]. However, in these studies the fiber orientation evolution

* Corresponding author at: Institute of Engineering Mechanics, Chair for Continuum Mechanics, Karlsruhe Institute of Technology (KIT), Kaiserstraße 10, 76131 Karlsruhe, Germany.
E-mail address: tobias.karl@kit.edu (T. Karl).

https://doi.org/10.1016/j.ijmecsci.2023.108771
Received 1 June 2023; Received in revised form 15 September 2023; Accepted 20 September 2023
Available online 22 September 2023

is only influenced by the flow field of the anisotropically modeled fiber suspension and the anisotropic microstructure of the fiber suspension is not considered in the fiber orientation evolution.

Gilormini and Chinesta [28] studied anisotropy effects on the evolution behavior of rod-like particles. They developed a dumbbell model for slender fibers embedded in an anisotropic suspension. The anisotropy represents the hydrodynamic interactions between the fibers arising with increasing fiber volume fraction. In their approach they used the viscous drag force in an incompressible suspension with fiber-induced orthotropic material symmetry for modeling the hydrodynamic interactions. The micromechanical model of Mori and Tanaka [29,30] and the IBOF closure [31] was used. The results of Gilormini and Chinesta show distinct differences between the classical Jeffery model [5,6] and the proposed anisotropic orientation model. The latter causes a stronger alignment with increasing fiber volume fraction (moderate) and fiber aspect ratio (distinct) in the shear direction with respect to the Jeffery model. In addition, the 2D case is briefly addressed referring to the work of Fletcher [32] with the result, that in 2D the anisotropy of the surrounding fluid does not affect the spin of the embedded fiber.

Favaloro [33], on the other hand, used the mean-field approaches of Reuss [34] and of Mori and Tanaka [29,30] to describe the motion of a single fiber embedded in an anisotropic fiber suspension. Based on this single-fiber consideration, the corresponding evolution equation for the second-order orientation tensor was derived by means of upscaling. Favaloro found that, in contrast to the Reuss model depending on the particle number, the Mori–Tanaka model leads to an additional term that scales with the fiber volume fraction and is in this sense consistent with the interaction models of Feréc et al. [35,36]. The results for a shear flow show the same behavior as the model of Gilormini and Chinesta [28], namely that the consideration of the volume fraction leads to a more pronounced orientation. In addition, it is shown by Favaloro [33] that the derived orientation evolution equations can be easily modified by an additional parameter similar to the RSC model [20] to account for slower orientation dynamics.

The study of Favaloro [33] is mainly based on the work of Wetzel and Tucker [37] with the underlying doctoral thesis of Wetzel [38]. Wetzel and Tucker [37] studied the deformation of an ellipsoidal Newtonian droplet embedded in a Newtonian matrix fluid for the first time in 3D. They used the compact localization tensor notation which is related to the basis of mean-field homogenization: Eshelby's single inclusion problem [39,40]. It should be noted that the approach of Wetzel and Tucker covers arbitrary flow conditions and fluid viscosities under Stokes flow conditions and neglects interfacial tension of the considered ellipsoidal droplet. In earlier works, e.g., Bilby et al. [41], Howard und Brierley [42] and Bilby und Kolbuszewski [43] the results of Eshelby were applied for special flows and under geometric restrictions of the droplet. A remarkable finding of Wetzel and Tucker is the mean-field based derivation of Jeffery's equation [5,6] assuming a rigid spheroidal particle and the localization tensor of the dilute distribution (see, e.g., Tucker and Liang [44]).

A recent publication of Ponte Castañeda [45] generalizes, e.g., the work of Avazmohammadi and Ponte Castañeda [46] in the context of the Hashin–Shtrikman–Willis approach [47,48] formulated by Ponte Castañeda and Willis [49] in order to describe the orientation and shape evolution of deformable ellipsoidal particles with different distributions and geometries. The embedded particles are considered viscoelastic or elasto-viscoplastic, whereas the fluid can show Newtonian or viscoplastic behavior. Since the present work is not focused on deformable particles, the reader is referred to the literature survey of Ponte Castañeda [45] for more details on this subject. As stated by Ponte Castañeda [45], the Jeffery equation follows as a special case for rigid particles in a Newtonian matrix fluid, provided a dilute distribution is assumed (see Wetzel and Tucker [37]).

Since the present work favors fast mean-field homogenization methods over computationally expensive full-field simulations for the formulation of fiber orientation evolution equations, a brief review of selected recent publications on mean-field homogenization of particle suspensions is given here. Full-field simulations, see, e.g., Schneider [50], Bertóti et al. [51], and Sterr et al. [52] are not part of this study as they require a fully resolved microstructure. Bertóti and Böhlke [53] used a two-step Hashin–Shtrikman approach for the special case of rigid spheroidal inclusions and simulated a fiber set governed by Jeffery's equation for each individual fiber. Regarding four different flow cases, both the orientation evolution and the evolution of the effective viscosity tensor were investigated. For the viscous stress evolution, the differences between the mean-field model and the constitutive law of Dinh and Armstrong [54] were studied. The results show that the chosen mean-field approach is sufficient to model the viscosity of the fiber suspension. Traxl et al. [55] formulated equations for four different matrix fluids and three different inclusion geometries, where both rigid particles and pores were considered. Karl and Böhlke [56] addressed various mean-field homogenization models in parallel for the estimation of effective viscous and elastic properties of fiber suspensions and composites. In the same study, the Hill–Mandel condition [57,58] for viscous suspensions was reconsidered in detail with respect to singular surfaces, complementing the work of, e.g., Adams and Field [59] and Traxl et al. [55]. Upper estimates were proposed in order to provide macroscopically non-rigid approximations leading to higher effective viscosities compared to the applied mean-field methods and lower bounds. Kammer et al. [60] generalized the homogenization approach of Ponte Castañeda and Willis [49] in order to approximate the effective viscosity of suspensions with isotropically distributed rigid spherical particles. Both Newtonian and viscoplastic matrix fluids were considered. An empirical scalar parameter was used to interpolate between the Ponte Castañeda and Willis estimates and self-consistent estimates [61,62]. It was shown that the proposed model agrees well with experimental results and that the empirical parameter can be interpreted as a representation of the polydisperse character of the particle suspension. Kammer and Ponte Castañeda [63] generalized the Ponte Castañeda-Willis approach [49] and the self-consistent estimate [61,62] in parallel by using the same empirical scalar parameter introduced by Kammer et al. [60] in order to interpolate between both methods. The further development of Kammer and Ponte Castañeda [63] includes a general tensorial approach with the additional feature of considering different inclusion geometries, mechanical behaviors of the constituents, orientations and distributions while fulfilling the necessary index symmetries of the effective tensors. In the context of the present work, reference is made to their results of estimating the effective linear viscous behavior for both a statistically isotropic distribution of rigid spheres and an isotropic distribution of rigid ellipsoidal fibers in a Newtonian matrix fluid.

1.2. Originality and structure

The aim of this work is to make an algebraic contribution to the description of the evolution of fiber orientation tensors taking into account the anisotropic viscosity induced by the local fiber orientation distribution. The focus is on the application of linear mean-field homogenization theory, which is widely used for solid composites. These methods are chosen because of their direct algebraic formulation and the possibility of efficient computation, which is of great importance in engineering practice. The two central points of the present work are summarized as follows:

(1) Based on a linear homogenization approach, the evolution equation of the fiber orientation tensor is formulated taking into account the anisotropic viscosity in such a way that variable mean-field models are applicable for the localization relations. From the point of view of a single fiber, this corresponds to a hydrodynamic interaction between the fiber and its environment, referring to an anisotropic suspension. In this context, the works of Wetzel [38], Wetzel and Tucker [37], Gilormini and

Chinesta [28] and Favaloro [33] are generalized. Specifically, the orientation evolution equations for four different mean-field models are specified and compared numerically for a simple shear flow.

(2) The fiber orientation tensor evolution equation is formulated for arbitrary even order, which is an additional algebraic generalization. The studies of Hill [64], Böhlke [65] and Papenfuss [66] are put into a new context in the sense of considering the anisotropic viscosity of the fiber suspension in this equation of arbitrary even order. In particular, it is shown how Jeffery's equation [5,6] and the Folgar–Tucker equation [18,19] for the orientation tensor of arbitrary even order follow from the general mean-field approach by proving the equivalence of the formulation for a single fiber to the work of Wetzel and Tucker [37].

The manuscript is structured as follows. Section 1 refers to the state of the art, the originality of the work and details about the notation. In Section 2 the basics for the description of fiber orientation states are presented. In addition, the mean-field based fiber orientation tensor evolution equation of arbitrary even order is formulated and specified for selected mean-field models. The special cases of the Jeffery equation and the Folgar–Tucker equation are discussed. Section 3 contains the results of a numerical example and the discussion. The summary and conclusions of the present study can be found in Section 4. Supplementary computations and additional results are provided in Appendix A to Appendix E. The supplementary material, which contains the list of symbols and abbreviations, can be found in Appendix F.

1.3. Notation

In this manuscript, a symbolic tensor notation is predominantly used. Where index notation is used, it refers to Cartesian index notation. Scalar quantities are denoted by lower and upper case Latin and Greek letters, e.g., a, A, α. Lower case bold letters are used for vectors, e.g., $\boldsymbol{a}, \boldsymbol{b}$. Second-order tensors are denoted by upper case bold Latin letters, e.g., $\boldsymbol{A}, \boldsymbol{B}$ and bold Greek letters, e.g., $\boldsymbol{\sigma}, \boldsymbol{\Omega}$. Fourth-order tensors refer to upper case blackboard bold Latin letters, e.g., $\mathbb{A}, \mathbb{B}$. Tensors of arbitrary order n are denoted by, e.g., $\mathbb{A}_{\langle n\rangle}, \mathbb{B}_{\langle n\rangle}$. The dyadic product between vectors and tensors is given by, e.g., $\boldsymbol{a}\otimes\boldsymbol{b}$. The abbreviation of the form $\boldsymbol{n}^{\otimes 2}$ refers to $\boldsymbol{n}\otimes\boldsymbol{n}$. The composition of second-order tensors refers to, e.g., $(\boldsymbol{AB})_{ij} = A_{ik}B_{kj}$ and of fourth-order tensors to, e.g., $(\mathbb{AB})_{ijkl} = A_{ijmn}B_{mnkl}$. The mapping of a second-order tensor over a fourth-order tensor is denoted by, e.g., $(\mathbb{A}[\boldsymbol{B}])_{ij} = A_{ijkl}B_{kl}$. The box product between second-order tensors is defined via $(\boldsymbol{A}\square\boldsymbol{B})_{ijkl} = A_{ik}B_{lj}$. The second-order identity tensor is denoted by $\boldsymbol{I}$. The identity on symmetric second-order tensors is given by $\mathbb{I}^{\mathrm{S}}$ and $\mathbb{I}^{\mathrm{A}}$ represents the identity on skew-symmetric second-order tensors, respectively. The tensor $\mathbb{P}_1$ stands for the identity on spherical second-order tensors whereas $\mathbb{P}_2$ represents the identity on symmetric traceless second-order tensors. Volume-averaged quantities are denoted by $\langle\cdot\rangle$ and effective quantities defined at the boundary of the considered volume element refer to $\bar{(\cdot)}$.

2. Fiber orientation tensor evolution

Section content. The following subsections form the main theoretical part of the study. First, the basics of the tensorial description of fiber orientation are presented. This is followed by the micromechanical derivation of the general evolution equation of the orientation tensor of arbitrary even order. This generalized formulation is specified for selected mean-field models which differ in the respective localization (or concentration) relation.

2.1. Fiber orientation description

The fiber orientation of a given microstructure is most comprehensively described by the orientation distribution function f, which is a probability density function with the following properties [18,67]

$$f(\boldsymbol{n}) \geq 0, \qquad \int_S f(\boldsymbol{n})\,\mathrm{d}S(\boldsymbol{n}) = 1, \qquad f(\boldsymbol{n}) = f(-\boldsymbol{n}). \tag{1}$$

The vector $\boldsymbol{n}$ refers to an arbitrary direction on the unit sphere S with the surface element $\mathrm{d}S(\boldsymbol{n})$. It should be noted that the notation $\mathrm{d}S(\boldsymbol{n})$ indicates that $\boldsymbol{n}$ represents the integration variable. As time-varying and inhomogeneous microstructures are considered throughout this work, the function f also depends on the time t and the spatial coordinate $\boldsymbol{x}$, which is not shown in Eq. (1) for clarity. As described by, e.g., Böhlke et al. [68], Müller and Böhlke [69] and Bauer and Böhlke [70] the function f refers to the infinitesimal volume fraction $\mathrm{d}v/v$ of fibers aligned in the direction $\boldsymbol{n}$

$$\frac{\mathrm{d}v}{v}(\boldsymbol{n}) = f(\boldsymbol{n})\,\mathrm{d}S(\boldsymbol{n}). \tag{2}$$

In engineering practice, fiber orientation tensors [17,18] are used to represent moments of the orientation distribution function f and refer to a coarse-grained representation of the microstructure. The orientation tensor of the first kind and of arbitrary even order n reads [17,18]

$$\mathbb{N}_{\langle n\rangle}(\boldsymbol{x}, t) = \int f(\boldsymbol{x}, t, \boldsymbol{n})\boldsymbol{n}^{\otimes n}\,\mathrm{d}S(\boldsymbol{n}). \tag{3}$$

A restriction to the second- and fourth-order orientation tensor $\boldsymbol{N}$ and $\mathbb{N}$ in order to reduce the computational effort in engineering practice leads to a loss of microstructural information, since the orientation distribution function f is approximated by a truncated series [17,18]. This series representation typically refers to the orientation tensors of the third kind for which reference is made to Kanatani [17]. Besides the approximation of f by a truncated series, function-based approaches can be used to reconstruct f. In this context, reference is made to the angular central Gaussian distribution (ACG) [71,72] or the Bingham distribution [73] forming the basis of the maximum entropy method [74–76]. In addition, it is possible to use an ellipse radius distribution [77], the Jeffery distribution [1] or non-orthotropic approaches [78]. To conclude this section it should be mentioned that the addressed fiber orientation description is only valid for rigid and thus non-curved short fibers.

2.2. Generalized formulation of the orientation evolution

As a starting point for deriving a generalized fiber orientation tensor evolution equation, the orientation average [18] (OA) of an arbitrary microstructural second-order tensor $\boldsymbol{A}(\boldsymbol{n})$ is considered

$$\langle\boldsymbol{A}\rangle_{\mathrm{OA}} = \int_S f(\boldsymbol{n}, t)\boldsymbol{A}(\boldsymbol{n})\,\mathrm{d}S(\boldsymbol{n}). \tag{4}$$

The argument $\boldsymbol{x}$ of f is omitted to ensure a more compact notation. Following the work of Böhlke [65] for polycrystals, the time derivative of $\langle\boldsymbol{A}\rangle_{\mathrm{OA}}$ is considered

$$\frac{\mathrm{d}}{\mathrm{d}t}\langle\boldsymbol{A}\rangle_{\mathrm{OA}} = \frac{\mathrm{d}}{\mathrm{d}t}\int_S f(\boldsymbol{n}, t)\boldsymbol{A}(\boldsymbol{n})\,\mathrm{d}S(\boldsymbol{n}). \tag{5}$$

As shown in Appendix A, Eq. (5) can be transformed into the following generalized evolution equation for the orientation tensor $\mathbb{N}_{\langle n\rangle}$ of arbitrary even order n by substituting the tensor $\boldsymbol{A}$ with $\boldsymbol{n}^{\otimes n}$

$$\dot{\mathbb{N}}_{\langle n\rangle} = \int_S f(\boldsymbol{n}, t)(\boldsymbol{n}^{\otimes n})^{\cdot}\,\mathrm{d}S(\boldsymbol{n}), \tag{6}$$

with the corresponding derivative

$$(\boldsymbol{n}^{\otimes n})^{\cdot} = \dot{\boldsymbol{n}}\otimes\boldsymbol{n}^{\otimes(n-1)} + \boldsymbol{n}\otimes\dot{\boldsymbol{n}}\otimes\boldsymbol{n}^{\otimes(n-2)} + \cdots + \boldsymbol{n}^{\otimes(n-1)}\otimes\dot{\boldsymbol{n}}. \tag{7}$$

It should be noted that the rate $\dot{\boldsymbol{n}}$ is a constitutive quantity when considering the analogous approach by Böhlke [65] for polycrystals.

Following Favaloro [33], the local fiber spin tensor $\boldsymbol{W}_{\mathsf{F}}$ is used in order to express the rate $\dot{\boldsymbol{n}} = \boldsymbol{W}_{\mathsf{F}}\boldsymbol{n}$. By using the fiber spin tensor $\boldsymbol{W}_{\mathsf{F}}$, the rate $(\boldsymbol{n}^{\otimes n})^{\cdot}$ is formally abbreviated by

$$(\boldsymbol{n}^{\otimes n})^{\cdot} = \boldsymbol{W}_{\mathsf{F}} \boxtimes (\boldsymbol{n}^{\otimes n}), \tag{8}$$

with the operator $\boxtimes$ defined via [65]

$$\begin{aligned}(\boldsymbol{n}^{\otimes n})^{\cdot}_{ijk\ldots l} &= W^{\mathsf{F}}_{im} n_m n_j n_k \ldots n_l + W^{\mathsf{F}}_{jm} n_i n_m n_k \ldots n_l \\ &\quad + W^{\mathsf{F}}_{km} n_i n_j n_m \ldots n_l + \cdots + W^{\mathsf{F}}_{lm} n_i n_j n_k \ldots n_m.\end{aligned} \tag{9}$$

As will be shown in the following part of the manuscript, $\boldsymbol{W}_{\mathsf{F}}$ and therefore the rate $(\boldsymbol{n}^{\otimes n})^{\cdot}$ depends on the effective spin, the local strain rate and the anisotropic environment of the fiber. With Eq. (8) the fiber orientation tensor evolution equation of arbitrary even order n can be compactly formulated as follows

$$\dot{\mathbb{N}}_{\langle n\rangle} = \int_{\mathcal{S}} f(\boldsymbol{n}, t) \boldsymbol{W}_{\mathsf{F}} \boxtimes (\boldsymbol{n}^{\otimes n}) \, \mathrm{d}S(\boldsymbol{n}). \tag{10}$$

It is noted that Eq. (10) is related to the generalized evolution equation for arbitrary statistical moments in terms of texture coefficients for polycrystals derived by Böhlke [65]. It is interesting to see that the algebraic structure is equal with respect to the set of orthogonal tensors SO3 and the unit sphere $\mathcal{S}$, and that the spin localization [59,79,80] is a crucial constitutive quantity that requires modeling.

In order to incorporate the microstructure into the evolution equation (10), the localization (or concentration) relation for the fiber spin tensor $\boldsymbol{W}_{\mathsf{F}}$ is addressed in the following. This serves as a starting point for the later application of arbitrary mean-field homogenization models. The approach of Adams and Field [59] is applied to viscous suspensions throughout this work, considering the quasi-static balance of linear momentum without volume forces, the constitutive law for linear viscous suspensions, the compatibility condition inside the volume V and the incompressibility condition

$$\boldsymbol{0} = \operatorname{div}(\boldsymbol{\sigma}), \qquad \boldsymbol{\sigma} = -p\boldsymbol{I} + \mathbb{V}[\boldsymbol{D}], \qquad \boldsymbol{0} = \operatorname{rot}(\operatorname{rot}^{\mathsf{T}}(\boldsymbol{D})), \qquad 0 = \operatorname{tr}(\boldsymbol{D}). \tag{11}$$

In the above system of equations, $\boldsymbol{\sigma}$ refers to the Cauchy stress tensor with the pressure p, the viscosity tensor $\mathbb{V}$, and the traceless strain-rate tensor $\boldsymbol{D}$ as the symmetric part of the velocity gradient $\boldsymbol{L}$. It is assumed that the constant macroscopic velocity gradient $\bar{\boldsymbol{L}}$ and the constant macroscopic pressure $\bar{p}$ are applied on the boundary ∂V [59]. The incompressible fiber suspension is assumed to be statistically homogeneous and ergodic [81] without cracks or voids and a continuous displacement or velocity field in the representative volume element [57]. The Hill–Mandel condition [57,58] for viscous suspensions and the underlying Stokes flow condition are assumed to be valid and only isotropic phases (fibers and matrix) with phase-wise uniform mechanical properties are considered [57]. In each homogenization step, the microstructure of the fiber suspension is seen as constant in time [45,56]. Based on the approach for linear elastic solids [48,82–85], a homogeneous reference viscosity $\mathbb{V}_0$ is introduced and the corresponding viscous stress polarization $\boldsymbol{\tau}$ and the constitutive law read

$$\boldsymbol{\tau} = (\mathbb{V} - \mathbb{V}_0)[\boldsymbol{D}], \qquad \boldsymbol{\sigma} = -p\boldsymbol{I} + \mathbb{V}_0[\boldsymbol{D}] + \boldsymbol{\tau}. \tag{12}$$

Using Eq. (12) the static balance of linear momentum without body forces can be reformulated for viscous suspensions similar to elastic solids, see, e.g., Willis [86], Lipinski and Berveiller [79] and Adams and Field [59]

$$\boldsymbol{0} = -\operatorname{grad}(p) + \operatorname{div}(\mathbb{V}_0[\boldsymbol{D}]) + \operatorname{div}(\boldsymbol{\tau}), \tag{13}$$

with the pressure boundary condition $p(\boldsymbol{x}) = \bar{p}$, $\boldsymbol{x} \in \partial V$ and the velocity boundary condition $\boldsymbol{v}(\boldsymbol{x}) = \bar{\boldsymbol{v}}$, $\boldsymbol{x} \in \partial V$. The formal solution of Eq. (13) can be expressed conveniently in index notation as follows with Green's functions $\boldsymbol{g}(\boldsymbol{x}, \boldsymbol{x}')$ and $\boldsymbol{G}(\boldsymbol{x}, \boldsymbol{x}')$ [59,79,86]

$$p(\boldsymbol{x}) = \bar{p} - \int_V \frac{\partial g_i(\boldsymbol{x}, \boldsymbol{x}')}{\partial x'_j} \tau_{ij}(\boldsymbol{x}') \, \mathrm{d}V(\boldsymbol{x}'),$$

$$v_i(\boldsymbol{x}) = \bar{v}_i - \int_V \frac{\partial G_{ik}(\boldsymbol{x}, \boldsymbol{x}')}{\partial x'_l} \tau_{kl}(\boldsymbol{x}') \, \mathrm{d}V(\boldsymbol{x}'), \tag{14}$$

with the boundary values $\boldsymbol{g}(\boldsymbol{x}, \boldsymbol{x}') = \boldsymbol{0}$, $\boldsymbol{x} \in \partial V$ and $\boldsymbol{G}(\boldsymbol{x}, \boldsymbol{x}') = \boldsymbol{0}$, $\boldsymbol{x} \in \partial V$. Since the pressure in the incompressible case only represents a reaction force, its calculation is not considered in the following. The components of the local velocity gradient $\boldsymbol{L}$ follow directly from the components of the local velocity $\boldsymbol{v}$ in Eq. (14) [79]

$$\begin{aligned}L_{ij}(\boldsymbol{x}) &= \bar{L}_{ij} - \int_V \frac{\partial^2 G_{ik}(\boldsymbol{x}, \boldsymbol{x}')}{\partial x'_l \partial x_j} \tau_{kl}(\boldsymbol{x}') \, \mathrm{d}V(\boldsymbol{x}') \\ &= \bar{L}_{ij} - \int_V \frac{\partial^2 G_{im}(\boldsymbol{x}, \boldsymbol{x}')}{\partial x'_n \partial x_j} I^{\mathsf{S}}_{mnkl} \tau_{kl}(\boldsymbol{x}') \, \mathrm{d}V(\boldsymbol{x}') \\ &= \bar{L}_{ij} - \int_V \Gamma_{ijkl}(\boldsymbol{x}, \boldsymbol{x}') \tau_{kl}(\boldsymbol{x}') \, \mathrm{d}V(\boldsymbol{x}').\end{aligned} \tag{15}$$

In the last step, the kernel of the integral is abbreviated by Γ_{ijkl} which is typically symmetrized in the right index pair leading to the compact notation of Eq. (15) similar to Willis [48,86]

$$\mathbb{\Gamma}\{\boldsymbol{\tau}\} : \boldsymbol{\tau} \mapsto \int_V \mathbb{\Gamma}(\boldsymbol{x}, \boldsymbol{x}')[\boldsymbol{\tau}(\boldsymbol{x}')] \, \mathrm{d}V(\boldsymbol{x}'), \qquad \boldsymbol{L}(\boldsymbol{x}) = \bar{\boldsymbol{L}} - \mathbb{\Gamma}\{\boldsymbol{\tau}\}. \tag{16}$$

In order to derive localization relations for the strain-rate tensor $\boldsymbol{D} = \operatorname{sym}(\boldsymbol{L})$ and for the spin tensor $\boldsymbol{W} = \operatorname{skw}(\boldsymbol{L})$, the integral operator $\mathbb{\Gamma}$ is either skew-symmetrized (A) or symmetrized (S) in the left index pair [59] which is denoted by $\mathbb{\Gamma}^{\mathsf{A}} = \mathbb{I}^{\mathsf{A}}\mathbb{\Gamma}$ and $\mathbb{\Gamma}^{\mathsf{S}} = \mathbb{I}^{\mathsf{S}}\mathbb{\Gamma}$, respectively. Similar to Eq. (16) one can write

$$\boldsymbol{D}(\boldsymbol{x}) = \bar{\boldsymbol{D}} - \mathbb{\Gamma}^{\mathsf{S}}\{\boldsymbol{\tau}\}, \qquad \boldsymbol{W}(\boldsymbol{x}) = \bar{\boldsymbol{W}} - \mathbb{\Gamma}^{\mathsf{A}}\{\boldsymbol{\tau}\}. \tag{17}$$

The integral operations of Eq. (17) can be transformed into linear mappings by taking into account the following points [48,86]:

(1) By considering an infinite volume V_∞ of a statistically homogeneous composite, $\mathbb{\Gamma}^{\mathsf{S,A}}(\boldsymbol{x}, \boldsymbol{x}')$ is replaced by the infinite translation-invariant operator $\mathbb{\Gamma}^{\mathsf{S,A}}_{\infty}(\boldsymbol{x}-\boldsymbol{x}')$. It should be noted that the superscript S,A represents an abbreviation meaning either S or A, not both in the sense of a composition.

(2) The localization relations (17) must fulfill $\langle \boldsymbol{D} \rangle = \bar{\boldsymbol{D}}$ and $\langle \boldsymbol{W} \rangle = \bar{\boldsymbol{W}}$ implying that the volume average of the integral operations vanishes: $\langle \mathbb{\Gamma}^{\mathsf{S}}\{\boldsymbol{\tau}\} \rangle = \boldsymbol{0}$ and $\langle \mathbb{\Gamma}^{\mathsf{A}}\{\boldsymbol{\tau}\} \rangle = \boldsymbol{0}$. This is ensured by defining the integral operator $\mathbb{\Gamma}^{\mathsf{S,A}}\{\boldsymbol{\tau}\}$ on the fluctuation field $\boldsymbol{\tau} - \langle \boldsymbol{\tau} \rangle$

$$\mathbb{\Gamma}^{\mathsf{S,A}}\{\boldsymbol{\tau}\} : \boldsymbol{\tau} \mapsto \int_V \mathbb{\Gamma}^{\mathsf{S,A}}_{\infty}(\boldsymbol{x} - \boldsymbol{x}')[\boldsymbol{\tau}(\boldsymbol{x}') - \langle \boldsymbol{\tau} \rangle] \, \mathrm{d}V(\boldsymbol{x}'). \tag{18}$$

(3) The viscous stress polarization $\boldsymbol{\tau}$ is assumed to be constant in each of the phases. If no long-range order and ellipsoidal two-point statistics are assumed, the integral operator (18) can be further simplified

$$\begin{aligned}\mathbb{\Gamma}^{\mathsf{S,A}}\{\boldsymbol{\tau}\} : \boldsymbol{\tau} &\mapsto \int_V \mathbb{\Gamma}^{\mathsf{S,A}}_{\infty}(\boldsymbol{x}) \, \mathrm{d}V(\boldsymbol{x})[\boldsymbol{\tau} - \langle \boldsymbol{\tau} \rangle], \\ \mathbb{P}^{\mathsf{S,A}}_0 &= \int_V \mathbb{\Gamma}^{\mathsf{S,A}}_{\infty}(\boldsymbol{x}) \, \mathrm{d}V(\boldsymbol{x}).\end{aligned} \tag{19}$$

The tensor $\mathbb{P}^{\mathsf{S,A}}_0$ is called polarization tensor and is either symmetric in the left index pair (S) or skew-symmetric (A) in the left index pair. It should be noted that both tensors $\mathbb{P}^{\mathsf{S,A}}_0$ are symmetric in the right index pair. Based on Eq. (19) the localization relations (17) read as the following linear mappings as derived by Adams and Field [59]

$$\boldsymbol{D} = \bar{\boldsymbol{D}} - \mathbb{P}^{\mathsf{S}}_0[\boldsymbol{\tau} - \langle \boldsymbol{\tau} \rangle], \qquad \boldsymbol{W} = \bar{\boldsymbol{W}} - \mathbb{P}^{\mathsf{A}}_0[\boldsymbol{\tau} - \langle \boldsymbol{\tau} \rangle], \tag{20}$$

which correspond to the expressions derived similarly by, e.g., Avazmohammadi and Ponte Castañeda [46] in the context of deformable particles in Newtonian fluids. The fiber spin tensor $\boldsymbol{W}_{\mathsf{F}}$ needed for Eq. (10) can be computed based on Eq. (20) as follows

$$\boldsymbol{W}_{\mathsf{F}} = \bar{\boldsymbol{W}} - \mathbb{P}^{\mathsf{A}}_0[\boldsymbol{\tau}_{\mathsf{F}} - \langle \boldsymbol{\tau} \rangle]. \tag{21}$$

For the special case of two-phase fiber suspensions the volume-averaged viscous stress polarization reads

$$\langle \boldsymbol{\tau} \rangle = c_{\mathsf{M}} \langle \boldsymbol{\tau} \rangle_{\mathsf{M}} + c_{\mathsf{F}} \langle \boldsymbol{\tau} \rangle_{\mathsf{F}}, \tag{22}$$

with the volume fraction of the matrix c_{M} and the fibers c_{F}. The homogeneous reference viscosity is set to the matrix viscosity $\mathbb{V}_0 = \mathbb{V}_{\mathsf{M}}$ leading to a vanishing polarization field in the matrix phase [46] and the volume average reads $\langle \boldsymbol{\tau} \rangle = c_{\mathsf{F}} \langle \boldsymbol{\tau} \rangle_{\mathsf{F}}$. The non-zero polarization field of the fiber phase

$$\boldsymbol{\tau}_{\mathsf{F}} = (\mathbb{V}_{\mathsf{F}} - \mathbb{V}_{\mathsf{M}})[\boldsymbol{D}_{\mathsf{F}}] = \delta\mathbb{V}[\boldsymbol{D}_{\mathsf{F}}] = \delta\mathbb{V}\mathbb{A}_{\mathsf{F}}[\bar{\boldsymbol{D}}] \tag{23}$$

depends on the strain-rate localization tensor $\mathbb{A}_{\mathsf{F}}$ of the fiber and the difference $\delta\mathbb{V} = \mathbb{V}_{\mathsf{F}} - \mathbb{V}_{\mathsf{M}}$. Herein, the local strain-rate tensor $\boldsymbol{D}_{\mathsf{F}}$ of the fiber is computed with the constant macroscopic strain-rate tensor $\bar{\boldsymbol{D}}$ via $\boldsymbol{D}_{\mathsf{F}} = \mathbb{A}_{\mathsf{F}}[\bar{\boldsymbol{D}}]$. As a result, the fiber spin tensor given in Eq. (21) can be computed as follows

$$\begin{aligned} \boldsymbol{W}_{\mathsf{F}} &= \bar{\boldsymbol{W}} - \mathbb{P}_0^{\mathsf{A}} \Big(\delta\mathbb{V}\mathbb{A}_{\mathsf{F}} - c_{\mathsf{F}} \langle \delta\mathbb{V}\mathbb{A} \rangle_{\mathsf{F}} \Big)[\bar{\boldsymbol{D}}] \\ &= \bar{\boldsymbol{W}} - \mathbb{P}_0^{\mathsf{A}} \delta\mathbb{V}\mathbb{A}_{\mathsf{F}}[\bar{\boldsymbol{D}}] + c_{\mathsf{F}} \mathbb{P}_0^{\mathsf{A}} \langle \delta\mathbb{V}\mathbb{A} \rangle_{\mathsf{F}}[\bar{\boldsymbol{D}}] \\ &= \bar{\boldsymbol{W}} - \boldsymbol{W}_{\mathsf{local}} + \bar{\boldsymbol{W}}_{\mathsf{mean}}. \end{aligned} \tag{24}$$

The first term $\bar{\boldsymbol{W}}$ refers to the macroscopic or far-field spin tensor of the flow, which is a constant contribution to the fiber spin tensor. The second term $\boldsymbol{W}_{\mathsf{local}}$ refers to an additional spin concentration according to Wetzel and Tucker [37]. Since only the macroscopic strain-rate tensor $\bar{\boldsymbol{D}}$ is involved, this term induces a local fiber spin depending on the local direction of the fiber even in the presence of spin-free macroscopic flow [37]. The third term $\bar{\boldsymbol{W}}_{\mathsf{mean}}$ contains the orientation average operator $\langle \cdot \rangle_{\mathsf{F}}$ introduced in Eq. (4) which accounts for the interaction between the fibers by considering the mean fiber orientation of the suspension as an anisotropic environment. It is noted that there is a constant contribution to the fiber spin only if the effective orientation itself is constant. However, in any real process, a single fiber does not have a constant anisotropic environment, as the flow generally changes the effective orientation over time. In addition, the third term also induces a spin even in the presence of spin-free macroscopic flow. The contributions $\boldsymbol{W}_{\mathsf{local}}$ and $\bar{\boldsymbol{W}}_{\mathsf{mean}}$ to the fiber spin tensor have different signs since together they define a fluctuation field of the spin which is derived from the convergence criterion of the integral operator in the context of Eq. (18). Whether $\boldsymbol{W}_{\mathsf{local}}$ and $\bar{\boldsymbol{W}}_{\mathsf{mean}}$ accelerate or decelerate the local spin with respect to $\bar{\boldsymbol{W}}$ depends in a complex way on the kinematics, the actual fiber direction and the mean orientation of the fiber suspension. The generalized fiber orientation evolution equation (10) can be specified by using the fiber spin tensor given in Eq. (24)

$$\begin{aligned} \dot{\mathbb{N}}_{\langle n \rangle} = \bar{\boldsymbol{W}} \boxtimes \mathbb{N}_{\langle n \rangle} &- \int_S f(\boldsymbol{n},t) \Big(\mathbb{P}_0^{\mathsf{A}} \delta\mathbb{V}\mathbb{A}_{\mathsf{F}}[\bar{\boldsymbol{D}}] \Big) \boxtimes (\boldsymbol{n}^{\otimes n}) \, \mathrm{d}S(\boldsymbol{n}) \\ &+ c_{\mathsf{F}} \int_S f(\boldsymbol{n},t) \Big(\mathbb{P}_0^{\mathsf{A}} \langle \delta\mathbb{V}\mathbb{A} \rangle_{\mathsf{F}}[\bar{\boldsymbol{D}}] \Big) \boxtimes (\boldsymbol{n}^{\otimes n}) \, \mathrm{d}S(\boldsymbol{n}). \end{aligned} \tag{25}$$

To conclude this section it should be noted that Eq. (25) is exact with regard to the assumptions addressed above and that the study is limited to a linear homogenization approach. The above evolution equation is not closed and the orientation distribution function f has to be estimated in engineering practice. In addition, the tensors $\mathbb{P}_0^{\mathsf{A}}$ and $\mathbb{A}_{\mathsf{F}}$ are approximated by using mean-field models. It is emphasized that Eq. (25) allows the application of arbitrary mean-field models for the localization tensor $\mathbb{A}_{\mathsf{F}}$, a selection of which are presented below.

2.3. Special case: Reconsideration of Jeffery's equation (J)

The motion of one single spheroidal rigid fiber in a Newtonian matrix fluid without Brownian motion, inertia effects and hydrodynamic interaction is covered by the Jeffery equation [5,6]. Since only one fiber is considered, the fiber spin tensor given in Eq. (24) can be simplified by applying $c_{\mathsf{F}} \to 0$

$$\boldsymbol{W}_{\mathsf{F}} = \bar{\boldsymbol{W}} - \mathbb{P}_0^{\mathsf{A}} \delta\mathbb{V}\mathbb{A}_{\mathsf{F}}[\bar{\boldsymbol{D}}]. \tag{26}$$

The suitable mean-field model for the localization tensor $\mathbb{A}_{\mathsf{F}}$ is the dilute distribution [37,38] which is also addressed in the following Section 2.4. As a result, the fiber spin tensor can be written as follows by using $\mathbb{A}_{\mathsf{F}}$ given in, e.g., Tucker and Liang [44]

$$\boldsymbol{W}_{\mathsf{F}} = \bar{\boldsymbol{W}} - \mathbb{P}_0^{\mathsf{A}} \delta\mathbb{V} \Big(\mathbb{I}^{\mathsf{S}} + \mathbb{P}_0^{\mathsf{S}} \delta\mathbb{V} \Big)^{-1} [\bar{\boldsymbol{D}}] = \bar{\boldsymbol{W}} - \mathbb{P}_0^{\mathsf{A}} \Big(\delta\mathbb{V}^{-1} + \mathbb{P}_0^{\mathsf{S}} \Big)^{-1} [\bar{\boldsymbol{D}}]. \tag{27}$$

The rigid fiber assumption $\mathbb{V}_{\mathsf{F}} \to \infty$ or, in other words, a vanishing fluidity $\delta\mathbb{V}^{-1}$ [51,56] leads to the following fiber spin tensor $\boldsymbol{W}_{\mathsf{F}}$ and to an equation for the rate $\dot{\boldsymbol{n}}$

$$\boldsymbol{W}_{\mathsf{F}} = \bar{\boldsymbol{W}} - \mathbb{P}_0^{\mathsf{A}} \Big(\mathbb{P}_0^{\mathsf{S}} \Big)^{-1} [\bar{\boldsymbol{D}}], \qquad \dot{\boldsymbol{n}} = \bar{\boldsymbol{W}} \boldsymbol{n} - \mathbb{P}_0^{\mathsf{A}} \Big(\mathbb{P}_0^{\mathsf{S}} \Big)^{-1} [\bar{\boldsymbol{D}}] \boldsymbol{n}. \tag{28}$$

It is shown in Appendix B that the polarization tensor-based notation of Eq. (28) corresponds to the following equivalent formulation of Wetzel [38] and Wetzel and Tucker [37]

$$\boldsymbol{W}_{\mathsf{F}} = \bar{\boldsymbol{W}} + \mathbb{J}_{\mathsf{F}}[\bar{\boldsymbol{D}}], \qquad \dot{\boldsymbol{n}} = \bar{\boldsymbol{W}} \boldsymbol{n} + \mathbb{J}_{\mathsf{F}}[\bar{\boldsymbol{D}}] \boldsymbol{n}, \tag{29}$$

with the tensor $\mathbb{J}_{\mathsf{F}}$ introduced as *Jeffery tensor* in the present manuscript

$$\mathbb{J}_{\mathsf{F}} = \frac{1}{2} \xi \Big(\boldsymbol{I} \square (\boldsymbol{n} \otimes \boldsymbol{n}) + \big(\boldsymbol{I} \square (\boldsymbol{n} \otimes \boldsymbol{n}) \big)^{\mathsf{T}_{\mathsf{R}}} - (\boldsymbol{n} \otimes \boldsymbol{n}) \square \boldsymbol{I} - \big((\boldsymbol{n} \otimes \boldsymbol{n}) \square \boldsymbol{I} \big)^{\mathsf{T}_{\mathsf{R}}} \Big). \tag{30}$$

In Eq. (30) the shape parameter $\xi = (\alpha^2 - 1)/(\alpha^2 + 1)$ of the fibers depends on the fiber aspect ratio α. Combining Eqs. (29) and (30) leads to the following common representation [37,38]

$$\begin{aligned} \boldsymbol{W}_{\mathsf{F}} &= \bar{\boldsymbol{W}} + \xi \Big((\bar{\boldsymbol{D}} \boldsymbol{n}) \otimes \boldsymbol{n} - \boldsymbol{n} \otimes (\bar{\boldsymbol{D}} \boldsymbol{n}) \Big), \\ \dot{\boldsymbol{n}} &= \bar{\boldsymbol{W}} \boldsymbol{n} + \xi \Big(\bar{\boldsymbol{D}} \boldsymbol{n} - (\boldsymbol{n} \otimes \boldsymbol{n} \otimes \boldsymbol{n})[\bar{\boldsymbol{D}}] \Big). \end{aligned} \tag{31}$$

Finally, the generalized Jeffery equation for the fiber orientation tensor of arbitrary even order n can be derived by using the fiber spin tensor $\boldsymbol{W}_{\mathsf{F}}$ given in Eq. (31) in Eq. (10) together with the fiber orientation tensor definition (3) leading to

$$\dot{\mathbb{N}}_{\langle n \rangle} = \bar{\boldsymbol{W}} \boxtimes \mathbb{N}_{\langle n \rangle} + \xi \Big(\bar{\boldsymbol{D}} \boxtimes \mathbb{N}_{\langle n \rangle} - n \mathbb{N}_{\langle n+2 \rangle}[\bar{\boldsymbol{D}}] \Big). \tag{32}$$

To conclude this section, the generalization of the Folgar–Tucker approach [18,19] is addressed. In order to model fiber interaction, the following diffusion term on the unit sphere [18,19,87] is considered at the level of the Fokker–Planck equation [88] for the orientation distribution function

$$D = C_{\mathrm{I}} \dot{\gamma} \Delta_S(f(\boldsymbol{n},t)). \tag{33}$$

The parameter C_{I} refers to the fiber interaction parameter, the generalized shear rate is represented by $\dot{\gamma}$ and $\Delta_S(\cdot)$ stands for the Laplacian on the unit sphere. The corresponding diffusion term (or interaction term) of order n can be obtained by integrating $D\boldsymbol{n}^{\otimes n}$ over the unit sphere

$$\mathbb{D}_{\langle n \rangle} = C_{\mathrm{I}} \dot{\gamma} \int_S \boldsymbol{n}^{\otimes n} \Delta_S(f(\boldsymbol{n},t)) \, \mathrm{d}S(\boldsymbol{n}). \tag{34}$$

By transferring the following equivalence for periodic functions $a(\boldsymbol{n})$ and $b(\boldsymbol{n})$ on the unit sphere [89]

$$\int_S a(\boldsymbol{n}) \Delta_S(b(\boldsymbol{n})) \, \mathrm{d}S(\boldsymbol{n}) = \int_S b(\boldsymbol{n}) \Delta_S(a(\boldsymbol{n})) \, \mathrm{d}S(\boldsymbol{n}), \tag{35}$$

the alternative formulation of the interaction term (34) reads

$$\mathbb{D}_{\langle n \rangle} = C_{\mathrm{I}} \dot{\gamma} \int_S f(\boldsymbol{n},t) \Delta_S(\boldsymbol{n}^{\otimes n}) \, \mathrm{d}S(\boldsymbol{n}). \tag{36}$$

The Laplacian on the unit sphere $\Delta_S(\boldsymbol{n}^{\otimes n})$ can be computed analytically using the rules of calculus on the unit sphere as shown in Appendix C for the special case of $n = 2$. Applying this procedure to the general case in Eq. (36) leads to the generalized Folgar–Tucker interaction term

$$\mathbb{D}_{\langle n \rangle} = 2 C_{\mathrm{I}} \dot{\gamma} \left(\frac{(n-1)n}{2} \mathrm{sym}(\boldsymbol{I} \otimes \mathbb{N}_{\langle n-2 \rangle}) - \left(n + \frac{(n-1)n}{2} \right) \mathbb{N}_{\langle n \rangle} \right), \tag{37}$$

defining the generalized Folgar–Tucker equation

$$\dot{\mathbb{N}}_{\langle n\rangle} = \bar{\boldsymbol{W}}\boxtimes\mathbb{N}_{\langle n\rangle} + \xi\Big(\bar{\boldsymbol{D}}\boxtimes\mathbb{N}_{\langle n\rangle} - n\mathbb{N}_{\langle n+2\rangle}[\bar{\boldsymbol{D}}]\Big) + \mathbb{D}_{\langle n\rangle}. \tag{38}$$

The present section is concluded with the following remarks:

(1) As described by, e.g., Papenfuss [66] the orientation of rigid-rod molecules in liquid crystals is related to the orientation of rigid fibers contained in fiber suspensions. Analogously, orientation tensors (or alignment tensors representing orientation tensors of the third kind [17]) as statistical moments of the underlying orientation distribution functions are used to describe the macroscopic orientation state.
(2) In terms of a complete reconstruction of the orientation distribution function from its statistical moments, Papenfuss [66] derived the evolution equation for the orientation tensor of arbitrary order for liquid crystals. Micro-level effects such as potentials and molecular interactions were excluded and the general equation includes components from flow, diffusion and nematic parts. Hill [64] considered rigid-rod molecules in liquid crystals analogously and also formulated the evolution equation for the statistical moment of arbitrary order. In contrast to Papenfuss [66], the equation of Hill [64] also contains components from an electric field, a magnetic field and a dipole field and thus considers additional effects on the micro level.
(3) The studies of Hill [64] and Papenfuss [66] generalize the collision tensor considered by Latz et al. [90] to an arbitrary tensor order. It should be noted that the collision tensor consists of two opposing mechanisms: Diffusion as a driving force towards an isotropic state and the nematic part forcing an alignment.
(4) The generalized Folgar–Tucker equation (38) derived in this manuscript is related in parts to the equations of Hill [64] and Papenfuss [66] and can be understood as their counterpart in the usual notation of the fiber community.

In the following, the interaction term (37) based on diffusion on the unit sphere is not considered since the micromechanical models addressed in the next sections are to be compared with the unmodified Jeffery equation (32).

2.4. Special case: Dilute distribution (DD)

Similar to the derivation of the Jeffery equation in Section 2.3, the strain-rate localization tensor of the dilute distribution model [44,56]

$$\mathbb{A}_{\mathrm{F}} = \Big(\mathbb{I}^{\mathrm{S}} + \mathbb{P}_0^{\mathrm{S}}\delta\mathbb{V}\Big)^{-1} \tag{39}$$

is used in the general expression (24) for the fiber spin tensor. The difference to the derivation of Jeffery's equation is that the volume fraction of the fibers $c_{\mathrm{F}} \ll 1$ is non-zero and the associated term is not neglected. Therefore, the spin localization for the dilute distribution model reads as follows after a slight modification

$$\boldsymbol{W}_{\mathrm{F}} = \bar{\boldsymbol{W}} - \mathbb{P}_0^{\mathrm{A}}\Big(\delta\mathbb{V}^{-1} + \mathbb{P}_0^{\mathrm{S}}\Big)^{-1}[\bar{\boldsymbol{D}}] + c_{\mathrm{F}}\Big\langle\mathbb{P}_0^{\mathrm{A}}\Big(\delta\mathbb{V}^{-1} + \mathbb{P}_0^{\mathrm{S}}\Big)^{-1}[\bar{\boldsymbol{D}}]\Big\rangle_{\mathrm{F}}. \tag{40}$$

Applying the assumption of rigid fibers with a vanishing fluidity $\delta\mathbb{V}^{-1}$ as before, the above expression equals

$$\boldsymbol{W}_{\mathrm{F}} = \bar{\boldsymbol{W}} - \mathbb{P}_0^{\mathrm{A}}\Big(\mathbb{P}_0^{\mathrm{S}}\Big)^{-1}[\bar{\boldsymbol{D}}] + c_{\mathrm{F}}\Big\langle\mathbb{P}_0^{\mathrm{A}}\Big(\mathbb{P}_0^{\mathrm{S}}\Big)^{-1}[\bar{\boldsymbol{D}}]\Big\rangle_{\mathrm{F}}. \tag{41}$$

Based on the considerations given in Appendix B, the above expression is equivalent to the following compact form

$$\boldsymbol{W}_{\mathrm{F}} = \bar{\boldsymbol{W}} + \mathbb{J}_{\mathrm{F}}[\bar{\boldsymbol{D}}] - c_{\mathrm{F}}\Big\langle\mathbb{J}_{\mathrm{F}}[\bar{\boldsymbol{D}}]\Big\rangle_{\mathrm{F}}, \tag{42}$$

with the Jeffery tensor $\mathbb{J}_{\mathrm{F}}$ given in Eq. (30) depending on the fiber aspect ratio and the direction of the spheroidal fiber. The operator $\langle\cdot\rangle_{\mathrm{F}}$ refers to Eq. (4) as the orientation average [18] and can be computed directly based on the convenient form of $\mathbb{J}_{\mathrm{F}}[\bar{\boldsymbol{D}}]$ with the second-order fiber orientation tensor $\boldsymbol{N}$

$$\boldsymbol{W}_{\mathrm{F}} = \bar{\boldsymbol{W}} + \xi\Big((\bar{\boldsymbol{D}}\boldsymbol{n})\otimes\boldsymbol{n} - \boldsymbol{n}\otimes(\bar{\boldsymbol{D}}\boldsymbol{n})\Big) - c_{\mathrm{F}}\xi\Big(\bar{\boldsymbol{D}}\boldsymbol{N} - \boldsymbol{N}\bar{\boldsymbol{D}}\Big). \tag{43}$$

It should be noted that the last term on the right-hand side represents a constant contribution (with respect to the fiber direction $\boldsymbol{n}$) to the fiber spin tensor for a given fiber orientation distribution and a macroscopic strain-rate tensor. In view of the orientation evolution of a single fiber

$$\dot{\boldsymbol{n}} = \bar{\boldsymbol{W}}\boldsymbol{n} + \xi\Big(\bar{\boldsymbol{D}}\boldsymbol{n} - (\boldsymbol{n}\otimes\boldsymbol{n}\otimes\boldsymbol{n})[\bar{\boldsymbol{D}}]\Big) - c_{\mathrm{F}}\xi\Big(\bar{\boldsymbol{D}}\boldsymbol{N} - \boldsymbol{N}\bar{\boldsymbol{D}}\Big)\boldsymbol{n} \tag{44}$$

it becomes clear that this constant tensor represents the anisotropic environment of a single fiber in a micromechanical sense. If it is taken into account that this term follows from $\mathbb{P}_0^{\mathrm{A}}[\langle\boldsymbol{\tau}\rangle]$ in Eq. (21) via $c_{\mathrm{F}}\mathbb{P}_0^{\mathrm{A}}\langle\delta\mathbb{V}\mathbb{A}\rangle_{\mathrm{F}}[\bar{\boldsymbol{D}}]$ in Eq. (24), it becomes apparent that the convergence criterion of the integral operator $\langle\mathbb{I}^{\mathrm{A}}\{\boldsymbol{\tau}\}\rangle = \boldsymbol{0}$ embodies the micromechanical interaction of a single fiber with its anisotropic environment (which is not represented in the Jeffery approach). In order to derive the evolution equation for the fiber orientation tensor of arbitrary even order n for the dilute distribution model, the fiber spin tensor (43) is used in Eq. (10). The resulting equation can be expressed as follows based on the fiber orientation tensor definition (3)

$$\dot{\mathbb{N}}_{\langle n\rangle} = \bar{\boldsymbol{W}}\boxtimes\mathbb{N}_{\langle n\rangle} + \xi\Big(\bar{\boldsymbol{D}}\boxtimes\mathbb{N}_{\langle n\rangle} - n\mathbb{N}_{\langle n+2\rangle}[\bar{\boldsymbol{D}}]\Big) - c_{\mathrm{F}}\xi\Big(\bar{\boldsymbol{D}}\boldsymbol{N} - \boldsymbol{N}\bar{\boldsymbol{D}}\Big)\boxtimes\mathbb{N}_{\langle n\rangle}. \tag{45}$$

2.5. Special case: Mori–Tanaka model (MT)

In case of the Mori–Tanaka mean-field model [29,30] the following strain-rate localization tensor is used for viscous suspensions [56,91,92]

$$\mathbb{A}_{\mathrm{F}} = \Big(\mathbb{I}^{\mathrm{S}} + c_{\mathrm{M}}\mathbb{P}_0^{\mathrm{S}}\delta\mathbb{V}\Big)^{-1}. \tag{46}$$

Following the computation steps already presented, the fiber spin tensor reads as follows

$$\boldsymbol{W}_{\mathrm{F}} = \bar{\boldsymbol{W}} - \mathbb{P}_0^{\mathrm{A}}\Big(\delta\mathbb{V}^{-1} + c_{\mathrm{M}}\mathbb{P}_0^{\mathrm{S}}\Big)^{-1}[\bar{\boldsymbol{D}}] + c_{\mathrm{F}}\Big\langle\mathbb{P}_0^{\mathrm{A}}\Big(\delta\mathbb{V}^{-1} + c_{\mathrm{M}}\mathbb{P}_0^{\mathrm{S}}\Big)^{-1}[\bar{\boldsymbol{D}}]\Big\rangle_{\mathrm{F}}, \tag{47}$$

which, for rigid fibers, can be simplified to

$$\boldsymbol{W}_{\mathrm{F}} = \bar{\boldsymbol{W}} - \frac{1}{c_{\mathrm{M}}}\mathbb{P}_0^{\mathrm{A}}\Big(\mathbb{P}_0^{\mathrm{S}}\Big)^{-1}[\bar{\boldsymbol{D}}] + \frac{c_{\mathrm{F}}}{c_{\mathrm{M}}}\Big\langle\mathbb{P}_0^{\mathrm{A}}\Big(\mathbb{P}_0^{\mathrm{S}}\Big)^{-1}[\bar{\boldsymbol{D}}]\Big\rangle_{\mathrm{F}}. \tag{48}$$

With the equality $\mathbb{J}_{\mathrm{F}} = -\mathbb{P}_0^{\mathrm{A}}\Big(\mathbb{P}_0^{\mathrm{S}}\Big)^{-1}$ shown in Appendix B, the above expression for the fiber spin tensor reads as follows with the orientation average operator $\langle\cdot\rangle_{\mathrm{F}}$ defined by Eq. (4)

$$\begin{aligned}\boldsymbol{W}_{\mathrm{F}} &= \bar{\boldsymbol{W}} + \frac{1}{c_{\mathrm{M}}}\mathbb{J}_{\mathrm{F}}[\bar{\boldsymbol{D}}] - \frac{c_{\mathrm{F}}}{c_{\mathrm{M}}}\Big\langle\mathbb{J}_{\mathrm{F}}[\bar{\boldsymbol{D}}]\Big\rangle_{\mathrm{F}}\\ &= \bar{\boldsymbol{W}} + \frac{\xi}{c_{\mathrm{M}}}\Big((\bar{\boldsymbol{D}}\boldsymbol{n})\otimes\boldsymbol{n} - \boldsymbol{n}\otimes(\bar{\boldsymbol{D}}\boldsymbol{n})\Big) - \frac{\xi c_{\mathrm{F}}}{c_{\mathrm{M}}}\Big(\bar{\boldsymbol{D}}\boldsymbol{N} - \boldsymbol{N}\bar{\boldsymbol{D}}\Big),\end{aligned} \tag{49}$$

which corresponds to Favaloro's [33] result in a different notation. The derivation of the rate $\dot{\boldsymbol{n}}$ regarding the direction of a single fiber embedded in an anisotropic suspension is straightforward. By using Eq. (49), the modified Jeffery equation based on the Mori–Tanaka model reads [33]

$$\dot{\boldsymbol{n}} = \bar{\boldsymbol{W}}\boldsymbol{n} + \frac{\xi}{c_{\mathrm{M}}}\Big(\bar{\boldsymbol{D}}\boldsymbol{n} - (\boldsymbol{n}\otimes\boldsymbol{n}\otimes\boldsymbol{n})[\bar{\boldsymbol{D}}]\Big) - \frac{\xi c_{\mathrm{F}}}{c_{\mathrm{M}}}\Big(\bar{\boldsymbol{D}}\boldsymbol{N} - \boldsymbol{N}\bar{\boldsymbol{D}}\Big)\boldsymbol{n}. \tag{50}$$

In the last step, the fiber spin tensor (49) is used in Eq. (10) in order to derive the evolution equation for the fiber orientation tensor of arbitrary even order

$$\dot{\mathbb{N}}_{\langle n\rangle} = \bar{\boldsymbol{W}}\boxtimes\mathbb{N}_{\langle n\rangle} + \frac{\xi}{c_{\mathrm{M}}}\Big(\bar{\boldsymbol{D}}\boxtimes\mathbb{N}_{\langle n\rangle} - n\mathbb{N}_{\langle n+2\rangle}[\bar{\boldsymbol{D}}]\Big) - \frac{\xi c_{\mathrm{F}}}{c_{\mathrm{M}}}\Big(\bar{\boldsymbol{D}}\boldsymbol{N} - \boldsymbol{N}\bar{\boldsymbol{D}}\Big)\boxtimes\mathbb{N}_{\langle n\rangle}. \tag{51}$$

It is noted that Eq. (51) generalizes the expression for the special case of order $n = 2$ given in Favaloro [33]. Furthermore, the derivation of Eq. (51) in the present paper differs by a generalized approach that allows the use of arbitrary mean-field models or arbitrary strain-rate localization tensors $\mathbb{A}_{\mathrm{F}}$.

2.6. Special case: Ponte Castañeda-Willis model (PCW)

The Ponte Castañeda-Willis model [49] is based on the idea of considering different inclusion geometries with different spatial distributions. In order to realize this, two different polarization tensors are introduced: One for the inclusion (i) and the other one for the spatial distribution (d). For the special case of one single inclusion geometry with one single distribution, both the skew symmetric (A) and symmetric (S) polarization tensor read [45]

$$\mathbb{P}_0^{\mathrm{A,S}} = \frac{1}{c_\mathrm{M}}\left(\mathbb{P}_\mathrm{i}^{\mathrm{A,S}} - c_\mathrm{F}\mathbb{P}_\mathrm{d}^{\mathrm{A,S}}\right). \tag{52}$$

Inserting the symmetric tensor given in Eq. (52) into the localization tensor of the Mori–Tanaka model, the localization tensor of the Ponte Castañeda-Willis model is obtained [45,49]

$$\mathbb{A}_\mathrm{F} = \left(\mathbb{I}^\mathrm{S} + \left(\mathbb{P}_\mathrm{i}^\mathrm{S} - c_\mathrm{F}\mathbb{P}_\mathrm{d}^\mathrm{S}\right)\delta\mathbb{V}\right)^{-1}. \tag{53}$$

The direct use of Eqs. (52) and (53) in the general expression (24) for the fiber spin tensor leads to the following results simplified for a vanishing fluidity $\delta\mathbb{V}^{-1}$ for rigid fibers

$$\begin{aligned}\boldsymbol{W}_\mathrm{F} = \bar{\boldsymbol{W}} &- \frac{1}{c_\mathrm{M}}\left(\mathbb{P}_\mathrm{i}^\mathrm{A} - c_\mathrm{F}\mathbb{P}_\mathrm{d}^\mathrm{A}\right)\left(\mathbb{P}_\mathrm{i}^\mathrm{S} - c_\mathrm{F}\mathbb{P}_\mathrm{d}^\mathrm{S}\right)^{-1}[\bar{\boldsymbol{D}}] \\ &+ \frac{c_\mathrm{F}}{c_\mathrm{M}}\left\langle\left(\mathbb{P}_\mathrm{i}^\mathrm{A} - c_\mathrm{F}\mathbb{P}_\mathrm{d}^\mathrm{A}\right)\left(\mathbb{P}_\mathrm{i}^\mathrm{S} - c_\mathrm{F}\mathbb{P}_\mathrm{d}^\mathrm{S}\right)^{-1}[\bar{\boldsymbol{D}}]\right\rangle_\mathrm{F}.\end{aligned} \tag{54}$$

It should be noted that Eq. (54) corresponds to the special case of one single inclusion geometry with one single distribution given in Ponte Castañeda [45] if rigid particles are considered and thus elastic components of the stress inside the particles are not present. However, in contrast, the spin localization (54) for this special case takes the anisotropic environment of the particle into account in an additional, orientation averaged term $\langle\cdot\rangle_\mathrm{F}$. This also results in a modified evolution equation (57) for the direction of a single fiber compared to the relation given in Ponte Castañeda [45] regarding deformable particles.

In the following, the additional spin tensor depending on the fiber direction

$$\boldsymbol{\Omega}(\boldsymbol{n}) = \left(\mathbb{P}_\mathrm{i}^\mathrm{A}(\boldsymbol{n}) - c_\mathrm{F}\mathbb{P}_\mathrm{d}^\mathrm{A}(\boldsymbol{n})\right)\left(\mathbb{P}_\mathrm{i}^\mathrm{S}(\boldsymbol{n}) - c_\mathrm{F}\mathbb{P}_\mathrm{d}^\mathrm{S}(\boldsymbol{n})\right)^{-1}[\bar{\boldsymbol{D}}] \tag{55}$$

is introduced for convenience. With this abbreviation at hand, the computation of the (constant) orientation averaged tensor in Eq. (54) representing the fiber's anisotropic environment can be expressed compactly as follows

$$\boldsymbol{\Omega}_\mathrm{OA} = \int_S f(\boldsymbol{p},t)\boldsymbol{\Omega}(\boldsymbol{p})\,\mathrm{d}S(\boldsymbol{p}). \tag{56}$$

It should be noted that the integration variable on the unit sphere is deliberately changed in $\boldsymbol{p}$ to avoid confusion with the fiber direction $\boldsymbol{n}$. Without any further simplifications being possible, the equation for the single fiber reads as follows

$$\dot{\boldsymbol{n}} = \bar{\boldsymbol{W}}\boldsymbol{n} - \frac{1}{c_\mathrm{M}}\boldsymbol{\Omega}(\boldsymbol{n})\boldsymbol{n} + \frac{c_\mathrm{F}}{c_\mathrm{M}}\boldsymbol{\Omega}_\mathrm{OA}\boldsymbol{n}. \tag{57}$$

A combination of Eq. (54) with Eq. (10) leads to the generalized evolution equation for the fiber orientation tensor of arbitrary even order for the Ponte Castañeda-Willis model

$$\dot{\mathbb{N}}_{\langle n\rangle} = \bar{\boldsymbol{W}}\boxtimes\mathbb{N}_{\langle n\rangle} - \frac{1}{c_\mathrm{M}}\int_S f(\boldsymbol{n},t)\boldsymbol{\Omega}(\boldsymbol{n})\boxtimes(\boldsymbol{n}^{\otimes n})\,\mathrm{d}S(\boldsymbol{n}) + \frac{c_\mathrm{F}}{c_\mathrm{M}}\boldsymbol{\Omega}_\mathrm{OA}\boxtimes\mathbb{N}_{\langle n\rangle}. \tag{58}$$

The present section is concluded with the following remarks:

(1) For the special case $\mathbb{P}_\mathrm{i}^{\mathrm{A,S}} = \mathbb{P}_\mathrm{d}^{\mathrm{A,S}}$, the strain-rate localization tensor (53) reduces to the Mori–Tanaka approach as described in the literature [49,93]. Therefore, also the orientation evolution equation (58) corresponds to the Mori–Tanaka approach (51) for this special case.

(2) For simplicity, it is possible to assume a spheroidal distribution of the fibers via an additional distribution aspect ratio α_d. Since the fibers are also modeled as spheroids with the aspect ratio $\alpha_\mathrm{i} = \alpha$, all four polarization tensors $\mathbb{P}_{\mathrm{i,d}}^{\mathrm{A,S}}$ can be computed identically. In Appendix D, an efficient computation procedure is shown avoiding an encapsulated integration over the unit sphere in the integral term of Eq. (58). As an alternative to a constant spheroidal distribution, an additional evolution equation for a distribution tensor can be solved [45], with a correspondingly adjusted computation of the polarization tensors $\mathbb{P}_\mathrm{d}^{\mathrm{A,S}}$.

(3) It should be noted that both aspect ratios $\alpha_{\mathrm{i,d}}$ referring to the assumption of both spheroidal fibers and distribution, cannot be chosen independently of each other. For a given fiber volume fraction c_F and a fiber geometry α_i, the following bounds for α_d must not be violated [49]

$$\alpha_\mathrm{d}^\mathrm{min} = \alpha_\mathrm{i}\sqrt{c_\mathrm{F}}, \qquad \alpha_\mathrm{d}^\mathrm{max} = \frac{\alpha_\mathrm{i}}{c_\mathrm{F}}. \tag{59}$$

(4) In consideration of the already shown connection between the Jeffery tensor $\mathbb{J}_\mathrm{F}$ and the polarization tensors $\mathbb{P}_0^{\mathrm{A,S}}$ via $\mathbb{J}_\mathrm{F} = -\mathbb{P}_0^\mathrm{A}\left(\mathbb{P}_0^\mathrm{S}\right)^{-1}$ (see Appendix B), one can conclude that the Ponte Castañeda-Willis model leads to the following *distribution-corrected Jeffery tensor*

$$\mathbb{J}_{\mathrm{F,d}} = -\left(\mathbb{P}_\mathrm{i}^\mathrm{A} - c_\mathrm{F}\mathbb{P}_\mathrm{d}^\mathrm{A}\right)\left(\mathbb{P}_\mathrm{i}^\mathrm{S} - c_\mathrm{F}\mathbb{P}_\mathrm{d}^\mathrm{S}\right)^{-1}. \tag{60}$$

This interpretation complements Ponte Castañeda's statement [45] that the special case of Jeffery's equation is included in the approach considered. This assumes $\mathbb{P}_\mathrm{i}^{\mathrm{A,S}} = \mathbb{P}_\mathrm{d}^{\mathrm{A,S}}$ and the limit $c_\mathrm{F} \to 0$. The present study builds on Ponte Castañeda's work [45] in the sense that a general evolution equation for the fiber orientation tensor of arbitrary order is derived which, unlike conventional approaches, takes into account the distribution of the fibers.

(5) Compared to the models previously considered, the intrinsic closure problem that the evolution equation for $\mathbb{N}_{\langle n\rangle}$ depends on the next higher order orientation tensor $\mathbb{N}_{\langle n+2\rangle}$ [18] is present in Eq. (58) in the form of an unknown orientation distribution function f. As already discussed in Section 2.1, function based approaches like the angular central Gaussian distribution (ACG) [71,72], the maximum entropy method [74–76] based on the Bingham distribution [73], the Jeffery distribution [1] or an ellipse radius distribution [77] can be used.

2.7. Special case: Effective medium approach (EM)

The last method considered in the present manuscript is the effective medium approach with the basic idea of embedding a single inclusion (dilute distribution) in a suspension with the (unknown) effective viscosity $\bar{\mathbb{V}}$ as described by, e.g., Kanaun and Levin [94]. As a result, the strain-rate localization tensor given in Eq. (39) reads [44,48,56,91]

$$\bar{\mathbb{A}}_\mathrm{F} = \left(\mathbb{I}^\mathrm{S} + \bar{\mathbb{P}}_0^\mathrm{S}\delta\bar{\mathbb{V}}\right)^{-1}, \tag{61}$$

with the abbreviation $\delta\bar{\mathbb{V}} = \mathbb{V}_\mathrm{F} - \bar{\mathbb{V}}$. Since the expression has the same algebraic structure as in the case of a dilute distribution and the fluidity $\delta\bar{\mathbb{V}}^{-1}$ also vanishes for rigid fibers, the fiber spin tensor reads as follows

$$\boldsymbol{W}_\mathrm{F} = \bar{\boldsymbol{W}} - \bar{\mathbb{P}}_0^\mathrm{A}\left(\bar{\mathbb{P}}_0^\mathrm{S}\right)^{-1}[\bar{\boldsymbol{D}}] + c_\mathrm{F}\left\langle\bar{\mathbb{P}}_0^\mathrm{A}\left(\bar{\mathbb{P}}_0^\mathrm{S}\right)^{-1}[\bar{\boldsymbol{D}}]\right\rangle_\mathrm{F}. \tag{62}$$

The polarization tensors $\bar{\mathbb{P}}_0^{\mathrm{A,S}}$ depend on the effective (in general anisotropic) viscosity tensor $\bar{\mathbb{V}}$ and must be computed by numerically integrating Eq. (D.1) in Appendix D. Therefore, no further simplifications of Eq. (62) are possible. With the additional spin tensor depending on the fiber direction

$$\bar{\boldsymbol{\Omega}}(\boldsymbol{n}) = \bar{\mathbb{P}}_0^\mathrm{A}(\boldsymbol{n})\left(\bar{\mathbb{P}}_0^\mathrm{S}(\boldsymbol{n})\right)^{-1}[\bar{\boldsymbol{D}}] \tag{63}$$

and with its (constant) orientation averaged representation

$$\bar{\boldsymbol{\Omega}}_{\mathsf{OA}} = \int_S f(\boldsymbol{p},t)\bar{\boldsymbol{\Omega}}(\boldsymbol{p})\,\mathrm{d}S(\boldsymbol{p}), \tag{64}$$

the evolution equation for a single fiber can be compactly expressed by

$$\dot{\boldsymbol{n}} = \bar{\boldsymbol{W}}\boldsymbol{n} - \bar{\boldsymbol{\Omega}}(\boldsymbol{n})\boldsymbol{n} + c_{\mathsf{F}}\bar{\boldsymbol{\Omega}}_{\mathsf{OA}}\boldsymbol{n}. \tag{65}$$

Again, the integration variable in Eq. (64) is changed to $\boldsymbol{p}$ to avoid confusion with the fiber direction $\boldsymbol{n}$. A combination of Eq. (62) with Eq. (10) leads to the following generalized orientation evolution equation of arbitrary even order based on the effective medium approach

$$\dot{\mathbb{N}}_{\langle n\rangle} = \bar{\boldsymbol{W}}\boxtimes\mathbb{N}_{\langle n\rangle} - \int_S f(\boldsymbol{n},t)\bar{\boldsymbol{\Omega}}(\boldsymbol{n})\boxtimes(\boldsymbol{n}^{\otimes n})\,\mathrm{d}S(\boldsymbol{n}) + c_{\mathsf{F}}\bar{\boldsymbol{\Omega}}_{\mathsf{OA}}\boxtimes\mathbb{N}_{\langle n\rangle}. \tag{66}$$

The present section is concluded with the following remarks:

(1) Similar to the PCW model, Eq. (66) is not closed since the orientation distribution function f is unknown. Based on suitable approaches listed in Section 2.6, the function f has to be approximated.

(2) In analogy to all previous considerations, in particular to Appendix B, the following *effective Jeffery tensor* can be defined

$$\mathbb{J}_{\mathsf{F}} = -\bar{\mathbb{P}}_0^{\mathsf{A}}\left(\bar{\mathbb{P}}_0^{\mathsf{S}}\right)^{-1}. \tag{67}$$

(3) Unlike the PCW model, it is not possible to avoid encapsulated integration in Eq. (66). In this context, encapsulated means that for each integration point on S in Eq. (66), two complete integrations over S must be performed to evaluate the tensor $\bar{\boldsymbol{\Omega}}(\boldsymbol{n})$ as given in Eq. (63).

(4) In contrast to all previously discussed orientation models, the effective viscosity tensor $\bar{\mathbb{V}}$ must be calculated explicitly in order to solve the orientation evolution equation (66). Below, the self-consistent method (SC) and the differential scheme (DS) are listed (see, e.g., Kanaun and Levin [94]) with the adaptation to fiber suspensions with rigid fibers [56]

$$\bar{\mathbb{V}}_{\mathsf{SC}} = \mathbb{V}_{\mathsf{M}} + c_{\mathsf{F}}\left\langle\left(\bar{\mathbb{P}}_0^{\mathsf{S}}\right)^{-1}\right\rangle_{\mathsf{F}}, \qquad \frac{\mathrm{d}\bar{\mathbb{V}}_{\mathsf{DS}}}{\mathrm{d}c_{\mathsf{F}}} = \frac{1}{1-c_{\mathsf{F}}}\left\langle\left(\bar{\mathbb{P}}_0^{\mathsf{S}}\right)^{-1}\right\rangle_{\mathsf{F}}. \tag{68}$$

It should be noted that, in general, Eq. (68) represents implicit expressions for the effective viscosity tensor $\bar{\mathbb{V}}$ and that Eq. (66) is not limited to these two methods.

(5) The computation of the effective viscosity based on Eq. (68) must be performed at each time step during the integration of Eq. (66). The fully explicit approach proves to be practical in order to decouple the computation of $\bar{\mathbb{V}}$ and $\mathbb{N}_{\langle n\rangle}$ in each time step since both tensors are coupled via the orientation distribution function in the orientation average of Eq. (68).

3. Numerical example and discussion

Section content. In this section, the numerical example of a simple shear flow is considered in order to investigate the results of the presented mean-field models. The orientation evolution equations for the second-order orientation tensor and for a single fiber are given, followed by a description of the relevant settings. Moreover, the component N_{11} of the orientation tensor $\boldsymbol{N}$ is plotted over the total shear. Additionally, the reorientation of a single fiber is shown. The fiber orientation predicted by the presented mean-field models is investigated in the context of slow orientation dynamics. Since the presented equations describing the evolution of the second-order fiber orientation tensor are not closed, the discussion addresses the problem of choosing a suitable closure method.

3.1. Considered orientation evolution equations

In order to examine the differences between the various mean-field models addressed above, the present section is limited to the following second-order equations for the evolution of the fiber orientation

$$\begin{aligned}
\dot{\boldsymbol{N}}_{\mathsf{J}} &= \bar{\boldsymbol{W}}\boldsymbol{N} - \boldsymbol{N}\bar{\boldsymbol{W}} + \xi\Big(\bar{\boldsymbol{D}}\boldsymbol{N} + \boldsymbol{N}\bar{\boldsymbol{D}} - 2\mathbb{N}[\bar{\boldsymbol{D}}]\Big),\\
\dot{\boldsymbol{N}}_{\mathsf{DD}} &= \bar{\boldsymbol{W}}\boldsymbol{N} - \boldsymbol{N}\bar{\boldsymbol{W}} + \xi\Big(\bar{\boldsymbol{D}}\boldsymbol{N} + \boldsymbol{N}\bar{\boldsymbol{D}} - 2\mathbb{N}[\bar{\boldsymbol{D}}]\Big)\\
&\quad - c_{\mathsf{F}}\xi\Big(\bar{\boldsymbol{D}}\boldsymbol{N}^2 + \boldsymbol{N}^2\bar{\boldsymbol{D}} - 2\boldsymbol{N}\bar{\boldsymbol{D}}\boldsymbol{N}\Big),\\
\dot{\boldsymbol{N}}_{\mathsf{MT}} &= \bar{\boldsymbol{W}}\boldsymbol{N} - \boldsymbol{N}\bar{\boldsymbol{W}} + \frac{\xi}{c_{\mathsf{M}}}\Big(\bar{\boldsymbol{D}}\boldsymbol{N} + \boldsymbol{N}\bar{\boldsymbol{D}} - 2\mathbb{N}[\bar{\boldsymbol{D}}]\Big)\\
&\quad - \frac{c_{\mathsf{F}}\xi}{c_{\mathsf{M}}}\Big(\bar{\boldsymbol{D}}\boldsymbol{N}^2 + \boldsymbol{N}^2\bar{\boldsymbol{D}} - 2\boldsymbol{N}\bar{\boldsymbol{D}}\boldsymbol{N}\Big),\\
\dot{\boldsymbol{N}}_{\mathsf{PCW}} &= \bar{\boldsymbol{W}}\boldsymbol{N} - \boldsymbol{N}\bar{\boldsymbol{W}} - \frac{1}{c_{\mathsf{M}}}\int_S f(\boldsymbol{n},t)\Big(\boldsymbol{\Omega}(\boldsymbol{n}\otimes\boldsymbol{n}) - (\boldsymbol{n}\otimes\boldsymbol{n})\boldsymbol{\Omega}\Big)\,\mathrm{d}S(\boldsymbol{n})\\
&\quad + \frac{c_{\mathsf{F}}}{c_{\mathsf{M}}}\Big(\boldsymbol{\Omega}_{\mathsf{OA}}\boldsymbol{N} - \boldsymbol{N}\boldsymbol{\Omega}_{\mathsf{OA}}\Big),\\
\dot{\boldsymbol{N}}_{\mathsf{EM}} &= \bar{\boldsymbol{W}}\boldsymbol{N} - \boldsymbol{N}\bar{\boldsymbol{W}} - \int_S f(\boldsymbol{n},t)\Big(\bar{\boldsymbol{\Omega}}(\boldsymbol{n}\otimes\boldsymbol{n}) - (\boldsymbol{n}\otimes\boldsymbol{n})\bar{\boldsymbol{\Omega}}\Big)\,\mathrm{d}S(\boldsymbol{n})\\
&\quad + c_{\mathsf{F}}\Big(\bar{\boldsymbol{\Omega}}_{\mathsf{OA}}\boldsymbol{N} - \boldsymbol{N}\bar{\boldsymbol{\Omega}}_{\mathsf{OA}}\Big),
\end{aligned} \tag{69}$$

It should be noted that the spin tensors $\boldsymbol{\Omega}$ and $\bar{\boldsymbol{\Omega}}$ depend on the integration variable $\boldsymbol{n}$. The respective definitions are given in Eq. (55) for the PCW model and in Eq. (63) for the EM approach. In addition, the following equations are solved in parallel with the Eqs. (69) to track a single fiber embedded in the fiber suspension

$$\begin{aligned}
\dot{\boldsymbol{n}}_{\mathsf{J}} &= \bar{\boldsymbol{W}}\boldsymbol{n} + \xi\Big(\bar{\boldsymbol{D}}\boldsymbol{n} - (\boldsymbol{n}\otimes\boldsymbol{n}\otimes\boldsymbol{n})[\bar{\boldsymbol{D}}]\Big),\\
\dot{\boldsymbol{n}}_{\mathsf{DD}} &= \bar{\boldsymbol{W}}\boldsymbol{n} + \xi\Big(\bar{\boldsymbol{D}}\boldsymbol{n} - (\boldsymbol{n}\otimes\boldsymbol{n}\otimes\boldsymbol{n})[\bar{\boldsymbol{D}}]\Big) - c_{\mathsf{F}}\xi\Big(\bar{\boldsymbol{D}}\boldsymbol{N} - \boldsymbol{N}\bar{\boldsymbol{D}}\Big)\boldsymbol{n},\\
\dot{\boldsymbol{n}}_{\mathsf{MT}} &= \bar{\boldsymbol{W}}\boldsymbol{n} + \frac{\xi}{c_{\mathsf{M}}}\Big(\bar{\boldsymbol{D}}\boldsymbol{n} - (\boldsymbol{n}\otimes\boldsymbol{n}\otimes\boldsymbol{n})[\bar{\boldsymbol{D}}]\Big) - \frac{\xi c_{\mathsf{F}}}{c_{\mathsf{M}}}\Big(\bar{\boldsymbol{D}}\boldsymbol{N} - \boldsymbol{N}\bar{\boldsymbol{D}}\Big)\boldsymbol{n},\\
\dot{\boldsymbol{n}}_{\mathsf{PCW}} &= \bar{\boldsymbol{W}}\boldsymbol{n} - \frac{1}{c_{\mathsf{M}}}\boldsymbol{\Omega}(\boldsymbol{n})\boldsymbol{n} + \frac{c_{\mathsf{F}}}{c_{\mathsf{M}}}\boldsymbol{\Omega}_{\mathsf{OA}}\boldsymbol{n},\\
\dot{\boldsymbol{n}}_{\mathsf{EM}} &= \bar{\boldsymbol{W}}\boldsymbol{n} - \bar{\boldsymbol{\Omega}}(\boldsymbol{n})\boldsymbol{n} + c_{\mathsf{F}}\bar{\boldsymbol{\Omega}}_{\mathsf{OA}}\boldsymbol{n}.
\end{aligned} \tag{70}$$

3.2. Settings

The numerical example is limited to a simple shear flow with the effective velocity gradient $\bar{\boldsymbol{L}} = \dot{\gamma}\,\boldsymbol{e}_1\otimes\boldsymbol{e}_2$, leading to the effective strain-rate tensor $\bar{\boldsymbol{D}}$ and spin tensor $\bar{\boldsymbol{W}}$

$$\bar{\boldsymbol{D}} = \dot{\gamma}\big(\boldsymbol{e}_1\otimes\boldsymbol{e}_2 + \boldsymbol{e}_2\otimes\boldsymbol{e}_1\big)/2, \qquad \bar{\boldsymbol{W}} = \dot{\gamma}\big(\boldsymbol{e}_1\otimes\boldsymbol{e}_2 - \boldsymbol{e}_2\otimes\boldsymbol{e}_1\big)/2. \tag{71}$$

All orientation evolution equations above are integrated with an explicit fourth-order Runge–Kutta method with the fixed time step $\Delta t = 0.05$ s. The isotropic initial condition $\boldsymbol{N}_0 = \boldsymbol{I}/3$ and the initial fiber direction $\boldsymbol{n}_0 = (1\ 1\ 1)^{\mathsf{T}}/\sqrt{3}\,\boldsymbol{e}_i$ is fixed. The evolution equations for the second-order orientation tensor are closed by using the ACG closure [71,72] with the tolerance 10^{-8}. The respective integration on the unit sphere is based on a Lebedev grid [95] using the implementation of Parrish [96]. For J, DD, MT and PCW, the maximum number of 5810 integration points is chosen, as this does not negatively affect the computation time. For the EM approach, which is limited to the differential scheme, 974 integration points are chosen in order to ensure a sufficiently high accuracy with a reasonable computational effort. The differential scheme is solved with an explicit fourth-order Runge–Kutta method with the fixed volume fraction step $\Delta c_{\mathsf{F}} = 0.01$ and the initial solution $\bar{\mathbb{V}}_0 = 3\mu_{\mathsf{v}}\mathbb{P}_1 + 2\mu_{\mathsf{s}}\mathbb{P}_2$. Similar to a previous study [56], the shear viscosity of the matrix is set to $\mu_{\mathsf{s}} = 1$ Pas and the matrix volume viscosity $\mu_{\mathsf{v}} = 10^6$ Pas is fixed. The solution

Table 1
For the selected mean-field models DD, MT, PCW and EM, the maximum values of the orientation tensor component N_{11} is given for different fiber volume fractions c_F. The maximum values of N_{11} refer to the considered interval of the total shear $\dot{\gamma}t \in [0, 30]$.

c_F	DD	MT	PCW(α_d^{min})	PCW(α_d^{max})	EM
0.02	0.881	0.917	0.947	0.916	0.826
0.05	0.855	0.930	0.968	0.928	0.812
0.1	0.826	0.948	0.979	0.944	0.795
0.15	0.805	0.962	0.983	0.957	0.782

of the differential scheme refers to the expression $\mathbb{P}_2\bar{\mathbb{V}}\mathbb{P}_2$ [56]. As an example, the fiber volume fraction c_F is varied between the values 0.02 and 0.15 and the fiber aspect ratio $\alpha = 10$ is fixed.[1] Due to the chosen fiber aspect ratio, the volume fractions correspond to the semi-concentrated regime ($\alpha^{-2} < c_F < \alpha^{-1} \Leftrightarrow 0.01 < c_F < 0.1$) and to the concentrated regime ($\alpha^{-1} \leq c_F \Leftrightarrow 0.1 \leq c_F$) according to Tucker [98]. It should be noted that, even for the concentrated regime, the present mean-field approach covers only a purely hydrodynamic interaction between the fibers, as stated by Ponte Castañeda [45]. For the PCW model, the aspect ratio of the inclusion α_i refers to $\alpha = 10$ and the distribution aspect ratios α_d^{min} and α_d^{max} are computed based on Eq. (59) for each fiber volume fraction. Typically $\alpha \to \infty$ is chosen, which is not done in the present work for the following reasons. On the one hand, it is to be investigated how the mean-field models affect the periodic orientation behavior, which is not present for the infinite aspect ratio $\alpha \to \infty$. On the other hand, for $\alpha \to \infty$ the distribution aspect ratios of the PCW model are infinite as well, which makes the PCW model equal to the MT model. Another arising issue is that $\alpha \to \infty$ leads to a singularity in the computation of the polarization tensor for anisotropic matrix viscosities according to Eq. (D.1) for the EM approach.

3.3. Results and discussion

In Fig. 1 the evolution of the fiber orientation tensor component N_{11} is shown with respect to the total shear $\dot{\gamma}t$. In the range of approximately $\dot{\gamma}t < 5$ it can be seen that the investigated models differ only slightly, while for the range of approximately $\dot{\gamma}t > 5$ a strongly different behavior can be seen. For the MT and PCW models, the maximum values of N_{11} increase with an increasing fiber volume fraction. This behavior corresponds to the tendency of recent studies [28,33]. For the DD and EM models, in contrast, a decrease of the maximum value of N_{11} can be seen with increasing fiber volume fraction. The maximum values of N_{11} with respect to the considered mean-field models and fiber volume fractions are given in Table 1. Furthermore, the PCW(α_d^{min}) model shows the least periodic reorientation behavior for the selected settings. In general, the orientation evolution is greatly influenced by the consideration of the spatial distribution of the fibers. With increasing fiber volume fraction, the period length for the MT and PCW(α_d^{max}) models increases, whereas the period length for the DD and EM models decreases. The evolution of the remaining components N_{22}, N_{33} and N_{12} is shown in Fig. E.4 in Appendix E.

The behavior of a single fiber embedded in the fiber suspension, whose effective orientation behavior is shown in Fig. 1, is discussed in the following. In Fig. 2a the orientation evolution of a single fiber is shown on the unit sphere for the fiber volume fraction $c_F = 0.15$ of the surrounding fiber suspension. Fig. 2b shows the projection of the orientation path on the $\boldsymbol{e}_1$–$\boldsymbol{e}_2$-plane. Although the total shear acting on the fiber is the same for all mean-field models considered, there are clear differences in the orientation behavior. These differences correspond to the effective behavior shown in Fig. 1. On the one hand, the longest path on the unit sphere is shown for DD and EM, which is related to the strongly pronounced periodic behavior visualized in Fig. 1. For MT and PCW(α_d^{max}), the weaker periodic behavior becomes apparent at the end of the path. For PCW(α_d^{min}), on the other hand, the largest period length of the reorientation is shown by the quasi-static final state in the considered total shear range. The result of the classical Jeffery equation, measured by path length, lies between the results of DD, EM and MT, PCW(α_d^{max}). The orientation evolution of a single fiber for all other considered fiber volume fractions is shown in Fig. E.5 in Appendix E.

It should be noted that the DD model is only valid in the dilute regime. Investigations with different fiber volume fractions showed that the results of DD already deviate significantly from those of the MT model for fiber volume fractions higher than 10^{-3}. The MT model shows the expected behavior of slowing down the orientation dynamics with increasing fiber volume fraction. The opposite behavior of DD shows that the respective linearized approach and the associated micromechanical assumption of non-interacting single fibers [44] is not appropriate and must be evaluated as non-physical. Interestingly, the application of the EM model shows qualitatively the same orientation dynamics and the periodic behavior is more sensitive to increasing fiber volume fractions compared to the DD model. What connects the DD and EM models is the similar basic structure of the orientation evolution equation. This can be recognized on the one hand by the linear scaling with the fiber volume fraction and on the other hand by the concept of the EM model, as a single inclusion is embedded in the medium with the effective viscosity. The observed amplifying effect of EM on the periodic reorientation can be attributed to the fact that the inherent self-consistent approach tends to overestimate the effective viscosity [56,91] by embedding rigid fibers in a viscous matrix compared to DD. In addition, the spin localization of the DD and EM models only includes the macroscopic strain rate, while the spin localization of MT, as a special case of PCW, is derived based on the effective matrix strain rate [29,30,44], which is shown in the present study to be crucial for the fiber orientation evolution.

To conclude the numerical example, the results of the derived mean-field based fiber orientation evolution equations in the context of slow orientation dynamics are briefly investigated. Based on the discussion above, the upcoming analysis is limited to the J, MT and PCW models for the selected fiber volume fractions. Following Favaloro [33], the observed slower orientation dynamics of real fiber suspensions is realized by using the reduction tensor $\mathbb{R}$ with the reduction parameter $\kappa \in [0, 1]$ and the right eigenvectors $\boldsymbol{r}_i$ of the second-order orientation tensor $\boldsymbol{N}$

$$\mathbb{R} = \mathbb{I}^S + (\kappa - 1) \sum_{i=1}^{3} \boldsymbol{r}_i \otimes \boldsymbol{r}_i \otimes \boldsymbol{r}_i \otimes \boldsymbol{r}_i . \tag{72}$$

The orientation dynamics predicted by the J, MT and PCW models are slowed down by the use of the reduced strain-rate tensor $\mathbb{R}[\bar{\boldsymbol{D}}]$ [33] instead of the unmodified strain-rate tensor $\bar{\boldsymbol{D}}$ in the respective orientation evolution equation. In this context, Jeffery's model (32) refers to the reduced-strain closure model (RSC) [20] with a neglected Folgar–Tucker fiber interaction term [18,19]. Fig. 3 shows the evolution of the fiber orientation tensor component N_{11} with respect to the total shear $\dot{\gamma}t$ for the exemplary reduction parameter $\kappa = 0.3$. Note that the smaller κ, the greater the slowdown effect. The results show that an increasing fiber volume fraction has a significant effect on the orientation evolution predicted by the slowed down mean-field models. Here, PCW(α_d^{min}) shows the least pronounced changes with increasing volume fraction, whereas the results of MT and PCW(α_d^{max}) strongly depend on the fiber volume fraction in the range of $\dot{\gamma}t > 40$. Analogous to Fig. 1, vanishing differences between the MT and PCW models are shown for large volume fractions and the effect of spatial distribution decreases, but is evaluated as significant in the context of slow orientation dynamics.

[1] For example, if Polypropylene is chosen as the matrix material and glass is chosen as the fiber material, then the fiber volume fraction of 0.02 to 0.15 corresponds to a fiber mass fraction of 0.05 to 0.33 based on the mass densities $\rho_M = 910\ \mathrm{kg/m^3}$ and $\rho_F = 2540\ \mathrm{kg/m^3}$ [97]. The highest volume fraction thus corresponds to the standard composite material PP-GF30.

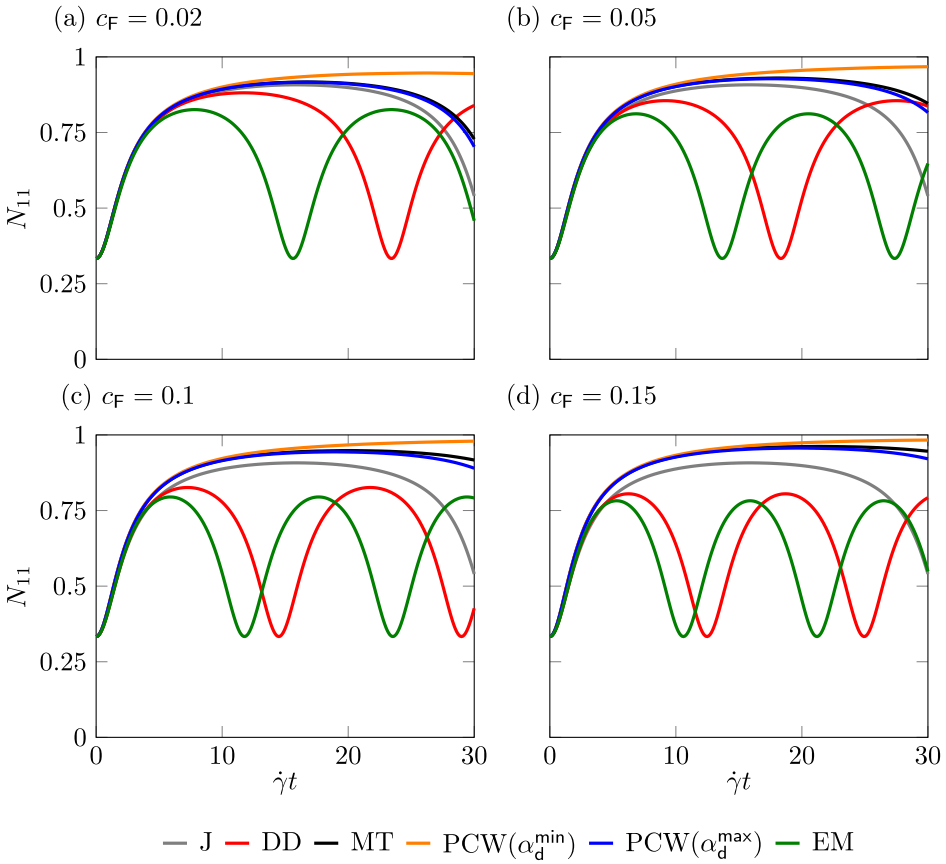

Fig. 1. For the selected mean-field models DD, MT, PCW and EM, the evolution of the orientation tensor component N_{11} in a simple shear flow is plotted over the total shear $\dot{\gamma}t$. The results of the Jeffery equation(J) are given for comparison. Different fiber volume fractions c_F are considered: 0.02 in (a), 0.05 in (b), 0.1 in (c) and 0.15 in (d). The legend is valid for all subplots.

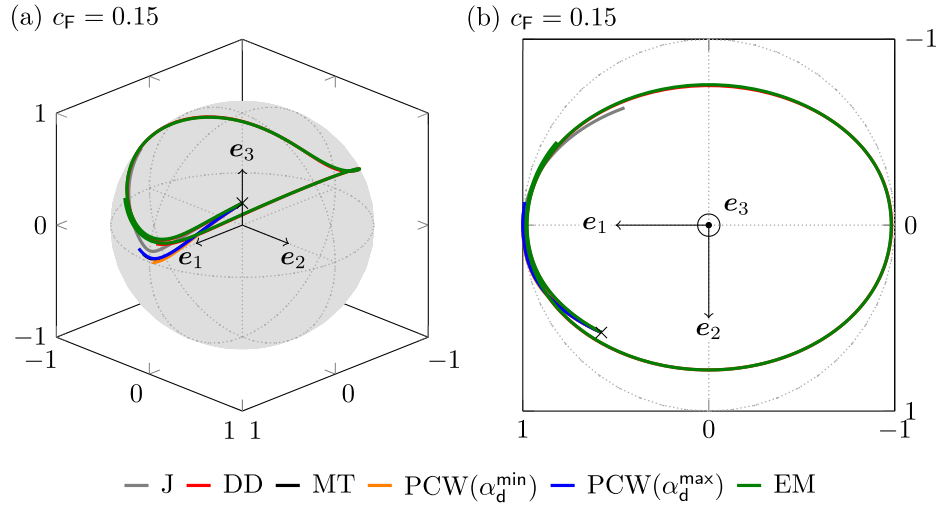

Fig. 2. For the fiber volume fraction $c_F = 0.15$ of the surrounding fiber suspension, the orientation behavior of a single fiber is shown for a simple shear flow with respect to the selected mean-field models DD, MT, PCW and EM. The Jeffery model (J) is considered as a reference. The initial fiber orientation is marked with ×. In (a), the orientation path of the single fiber is plotted on the unit sphere. The respective projection on the e_1–e_2-plane is shown in (b). The legend is valid for all subplots.

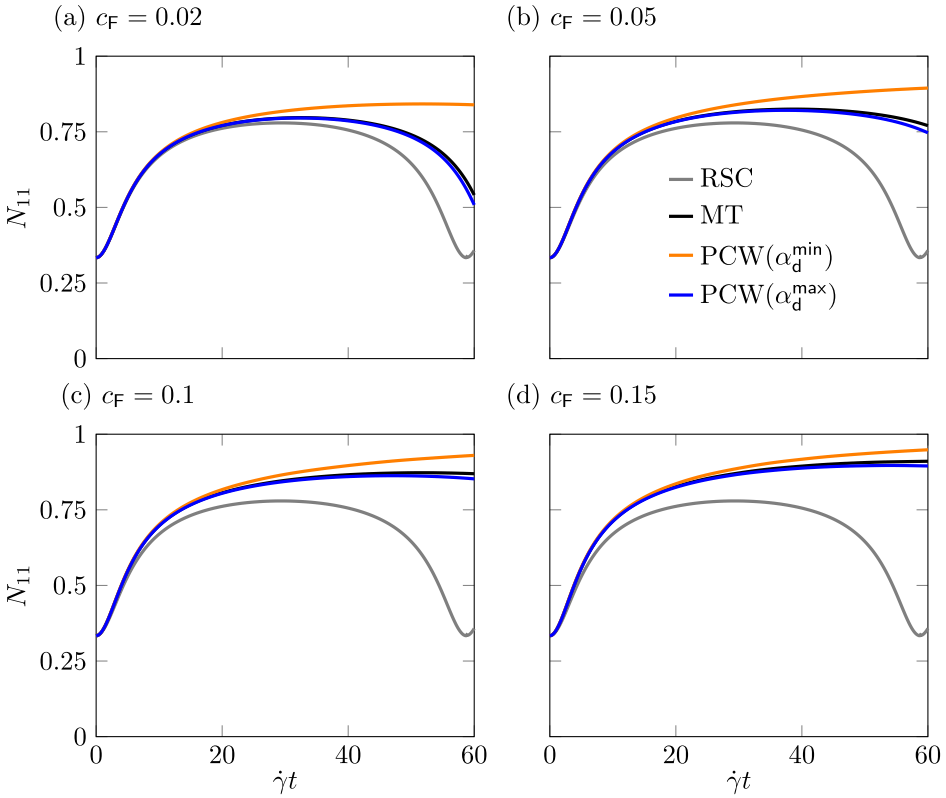

Fig. 3. For the selected mean-field models MT and PCW, the evolution of the orientation tensor component N_{11} in a simple shear flow is plotted over the total shear $\dot{\gamma}t$. The reduction parameter $\kappa = 0.3$ is used for slowing down the orientation dynamics. The results of the reduced-strain closure model without fiber interaction (RSC) are given for comparison. Different fiber volume fractions c_F are considered: 0.02 in (a), 0.05 in (b), 0.1 in (c) and 0.15 in (d). The legend is valid for all subplots.

3.4. Discussion of the closure problem

In the present work, the ACG closure [71,72] is assumed to be valid. As discussed by Favaloro [33] it should be noted that common closures for the micromechanically motivated new orientation equations do not necessarily lead to the same quality of results as known from the conventional orientation equations. Precise quantitative statements about how much the predicted orientation state varies when using different closures based on the reconstruction of the orientation distribution function f require extensive parameter studies. For the maximum entropy closure [74–76] based on the Bingham distribution [73], oscillations are expected in a simple shear flow as described by Tucker [78] and Karl et al. [99]. Based on the results given in Nabergoj et al. [77] for a simple shear flow, it can be concluded that the ellipse radius closure behaves qualitatively similar to the IBOF closure [31] with slight quantitative deviations from the predicted alignment. This observation can be transferred to the ACG closure, since the IBOF closure is an approximation of the ACG closure [31].

Future work could address the issue of finding an appropriate closure method and also consider the Jeffery distribution [1], as well as non-orthotropic approaches [78], which are so far only known for planar orientation states. There are two possible approaches to assessing the suitability of a closure for the mean-field based orientation evolution equations derived in this work. On the one hand, Favaloro's approach [33] can be used, where the orientation evolution of a statistically representative ensemble of single fibers is considered. Since the single-fiber equations do not require a closure, a comparison of the averaged orientation state can be made with, for example, the orientation state predicted by the second-order orientation evolution equations using a specific closure. On the other hand, a closure can be evaluated using the higher-order evolution equations derived in this work. The idea here is to use a specific closure approach and compare the higher-order orientation state at the end of the time integration with a reconstruction of this tensor using the time integration result of a lower-order evolution equation.

In order to identify a reliable combination of mean-field modeling and a closure method, further studies need to be carried out in the context of comparing numerical with experimental results. Future research should focus on implementing the derived evolution equations in mold-filling software and comparing the numerical results of the mean-field models with measured fiber orientation states in manufactured parts. In this context, specific extensions of the models can be considered in order to be in line with experimental data. A pragmatic first step would be to add the isotropic diffusion term similar to the classical Folgar–Tucker equation (38) and to fit the interaction parameter C_I to the experimental results. Therefore, the present work can serve as a basis for the development of micromechanically motivated and practical orientation models taking into account the anisotropic fiber suspension.

4. Summary and conclusions

The present paper deals with the micromechanical foundation of fiber orientation tensor evolution equations and presents a novel formula (25) for the evolution of orientation tensors of arbitrary even

order. Using a linear homogenization approach, the general orientation evolution formula is derived in a first step and allows the application of a variable mean-field models via the corresponding strain-rate localization tensor. Thus, the anisotropic character of the incompressible fiber suspension is algebraically taken into account in the evolution equation, which is an extension of the classical approach of Jeffery [5,6] and, e.g., Folgar and Tucker [18,19]. In a second step, the evolution equations are specified for the dilute distribution model (DD) [44], the Mori–Tanaka model (MT) [29,30], the approach of Ponte Castañeda and Willis (PCW) [49] and for the effective medium approach (EM) [94]. Both Jeffery's equation and the Folgar–Tucker equation of arbitrary tensor order are addressed as special cases of the formulated generalized mean-field approach and discussed in the literature context [37,38,64,66]. The present work is limited to rigid spheroidal short fibers embedded in a Newtonian matrix fluid under Stokes flow conditions. Brownian motion and inertia effects are not taken into account. The interaction between the fibers is modeled hydrodynamically by the chosen mean-field approach [45].

In the following, the conclusions of the present study are summarized and grouped thematically:

Orientation dynamics and application. For industrially relevant fiber volume fractions, DD leads to non-physical orientation dynamics and cannot be recommended. Not only because of the high computational cost of the EM model due to the encapsulated integration over the unit sphere, but also because the results of the EM model are similar to those of the DD model, EM cannot be recommended for engineering practice. For relevant fiber volume fractions and neglected spatial distribution of the fibers, the MT model is recommended. This is justified by the fact that with this model the common engineering approach $\alpha \to \infty$ can be used and that the MT approach is valid for higher fiber volume fractions. In addition, the periodic behavior is not present for $\alpha \to \infty$. In contrast, the PCW approach has the additional advantage over the MT model that the spatial distribution of the fibers is taken into account in the derived orientation tensor evolution equation. Furthermore, for relevant fiber volume fractions (e.g. $c_F > 0.1$) the PCW($\alpha_d^{\min}$) model shows a weak periodic orientation behavior for finite fiber aspect ratios and can therefore be recommended for predicting alignment under spatial distribution effects. The effects of the spatial distribution itself are rated as significant and their consideration opens up the possibility of a new way of computing the evolution of fiber orientation tensors. For engineering applications, one could consider stabilizing the weak periodic behavior of the PCW($\alpha_d^{\min}$) model by a very small Folgar–Tucker fiber interaction term in the sense of an artificial diffusion term. This would have the advantages that fitting of this additional term to experimental data would be possible and that micromechanical effects including the spatial distribution of the embedded fibers could be taken into account in the derived orientation evolution equations.

Slow orientation dynamics. The proposed micromechanical approach can serve as a basis for understanding the mechanics behind phenomenological models, such as the reduced-strain closure model (RSC) [20] or the anisotropic rotary diffusion model (ARD) [21]. In the present study, slowed orientation dynamics are investigated in the context of different mean-field models by using a modified strain-rate tensor [33]. Herein, the derived equations can be seen as a generalization of the reduced-strain closure model (RSC) [20] based on a consistent micromechanical approach that takes into account the anisotropic behavior of fiber suspensions. The investigation of a simple shear flow shows that the predicted fiber orientation strongly depends on the fiber volume fraction. In addition, the mean-field model itself plays an important role, where the consideration of the spatial distribution of the fibers in the evolution equation can be considered as crucial.

Micromechanical foundation of the Jeffery tensor. From an algebraic point of view, the present work shows that the Jeffery tensor $\mathbb{J}_F$, which localizes the additional contribution to the spin tensor $\mathbb{J}_F[\bar{\boldsymbol{D}}]$ and leads to Jeffery's equation (31), is related to the skew-symmetric (A) and symmetric (S) polarization tensors $\mathbb{P}_0^A$ and $\mathbb{P}_0^S$. The work of Wetzel [38] and Wetzel and Tucker [37] is thus complemented in that the Jeffery equation is derived from the general mean-field formulation considered in the present study. For the PCW model the distribution corrected Jeffery tensor $\mathbb{J}_{F,d}$ and for the EM model the effective Jeffery tensor $\bar{\mathbb{J}}_F$ are specified in this context in the present work.

Algebraic interpretation of the anisotropic interaction term. The general micromechanical formulation of the fiber orientation evolution equation (25) in this work allows the interpretation that the consideration of the anisotropic environment of the fiber or, in other words, the anisotropic interaction between fibers is related to the convergence criterion of the integral operator $\langle \mathbb{T}^A\{\boldsymbol{\tau}\}\rangle = \mathbf{0}$ in the context of the spin localization relation (17) and Eq. (18).

CRediT authorship contribution statement

Tobias Karl: Conceptualization, Methodology, Formal analysis, Investigation, Software, Data curation, Visualization, Writing – original draft, Writing – review & editing. **Thomas Böhlke:** Conceptualization, Supervision, Discussion, Funding acquisition, Writing – review & editing. All authors read and approved the manuscript.

Declaration of competing interest

The authors declare that they have no known competing financial interests or personal relationships that could have appeared to influence the work reported in this paper.

Data availability

Data will be made available upon reasonable request.

Acknowledgments

The partial financial support by the Friedrich und Elisabeth Boysen-Stiftung (Grant BOY-163) is gratefully acknowledged. The authors thank the anonymous reviewers for their insightful comments and suggestions.

Appendix A. Supplement to the generalized orientation evolution equation

Using Eq. (5) as a starting point, the derivation of Eq. (6) representing the generalized evolution equation for the orientation tensor $\mathbb{N}_{\langle n\rangle}$ of arbitrary even order n is given in the following. Eq. (5) can be reformulated with respect to the reference orientation distribution by using the reorientation gradient $\boldsymbol{F}_S \in \mathrm{Inv}^+$ on the unit sphere similar to the polycrystals-considering works of Kumar and Dawson [100] and Böhlke [65]

$$\boldsymbol{F}_S = \frac{\partial \boldsymbol{n}}{\partial \boldsymbol{n}_0} = \frac{\partial \chi_S(\boldsymbol{n}_0, t)}{\partial \boldsymbol{n}_0}. \tag{A.1}$$

In Eq. (A.1) the function χ_S maps the reference orientation $\boldsymbol{n}_0$ to the actual orientation $\boldsymbol{n}$ via $\boldsymbol{n} = \chi_S(\boldsymbol{n}_0, t)$. The relation between $f(\boldsymbol{n}, t)$ and the reference distribution $f_0(\boldsymbol{n}_0)$

$$f(\boldsymbol{n}, t) = \boldsymbol{J}_S^{-1} f_0(\boldsymbol{n}_0) \tag{A.2}$$

is implied by Eq. (2) based on the transformation rule of surface elements on the unit sphere reading $\mathrm{d}S(\boldsymbol{n}) = \boldsymbol{J}_S\, \mathrm{d}S_0(\boldsymbol{n})$ with the so-called

Jacobian determinant J_S of the reorientation [100]. As a consequence, Eq. (5) reads in the reference orientation

$$\begin{aligned}\frac{\mathrm{d}}{\mathrm{d}t}\langle\boldsymbol{A}\rangle_{\mathrm{OA}} &= \frac{\mathrm{d}}{\mathrm{d}t}\int_S J_S^{-1} f_0(\boldsymbol{n}_0)\boldsymbol{A}(\boldsymbol{n})J_S\,\mathrm{d}S_0(\boldsymbol{n})\\ &= \frac{\mathrm{d}}{\mathrm{d}t}\int_S f_0(\boldsymbol{n}_0)\boldsymbol{A}(\chi_S(\boldsymbol{n}_0,t))\,\mathrm{d}S_0(\boldsymbol{n}),\end{aligned} \tag{A.3}$$

whose time derivative is straightforward to compute by using the chain rule

$$\frac{\mathrm{d}}{\mathrm{d}t}\langle\boldsymbol{A}\rangle_{\mathrm{OA}} = \int_S f_0(\boldsymbol{n}_0)\frac{\partial\boldsymbol{A}}{\partial\chi_S}\frac{\partial\chi_S}{\partial t}\,\mathrm{d}S_0(\boldsymbol{n}). \tag{A.4}$$

The transformation of Eq. (A.4) into the actual orientation leads to the desired formulation

$$\begin{aligned}\frac{\mathrm{d}}{\mathrm{d}t}\langle\boldsymbol{A}\rangle_{\mathrm{OA}} &= \int_S J_S f(\boldsymbol{n},t)\frac{\partial\boldsymbol{A}}{\partial\boldsymbol{n}}\dot{\boldsymbol{n}}\,\mathrm{d}S_0(\boldsymbol{n})\\ &= \int_S f(\boldsymbol{n},t)\frac{\partial\boldsymbol{A}}{\partial\boldsymbol{n}}\dot{\boldsymbol{n}}\,\mathrm{d}S(\boldsymbol{n})\\ &= \int_S f(\boldsymbol{n},t)\dot{\boldsymbol{A}}(\boldsymbol{n})\,\mathrm{d}S(\boldsymbol{n}).\end{aligned} \tag{A.5}$$

With Eq. (A.5) at hand, the generalized evolution equation for the orientation tensor $\mathbb{N}_{\langle n\rangle}$ of arbitrary even order n is derived by substituting the tensor $\boldsymbol{A}$ in Eq. (A.5) with $\boldsymbol{n}^{\otimes n}$ leading to

$$\dot{\mathbb{N}}_{\langle n\rangle} = \int_S f(\boldsymbol{n},t)(\boldsymbol{n}^{\otimes n})^{\cdot}\,\mathrm{d}S(\boldsymbol{n}). \tag{A.6}$$

Appendix B. Supplement to the Jeffery equation

As a supplement to Section 2.3 it is formally shown in the following that under the assumptions made, the Jeffery equation (31) follows from the general spin localization (24). Methodically, the equivalence of the formulation (28) with the result (29) of Wetzel [38] and Wetzel and Tucker [37] is proven. The Jeffery tensor $\mathbb{J}_{\mathsf{F}}$ is called *vorticity concentration tensor* in the underlying studies [37,38] and reads

$$\mathbb{J}_{\mathsf{F}} = \left(1-\frac{\mu_{\mathsf{F}}}{\mu_{\mathsf{M}}}\right)\mathbb{E}^{\mathsf{A}}\left(\mathbb{I}^{\mathsf{S}}-\left(1-\frac{\mu_{\mathsf{F}}}{\mu_{\mathsf{M}}}\right)\mathbb{E}^{\mathsf{S}}\right)^{-1}, \tag{B.1}$$

with the so-called alternative Eshelby tensor $\mathbb{E}^{\mathsf{A}}$ and the common Eshelby tensor $\mathbb{E}^{\mathsf{S}}$. The shear viscosities of the matrix and the fibers refer to μ_{M} and μ_{F}. A simple modification of Eq. (B.1) leads to the following equivalent representation

$$\mathbb{J}_{\mathsf{F}} = -\mathbb{E}^{\mathsf{A}}\frac{1}{2\mu_{\mathsf{M}}}\left(2\mu_{\mathsf{F}}-2\mu_{\mathsf{M}}\right)\left(\mathbb{I}^{\mathsf{S}}+\mathbb{E}^{\mathsf{S}}\frac{1}{2\mu_{\mathsf{M}}}\left(2\mu_{\mathsf{F}}-2\mu_{\mathsf{M}}\right)\right)^{-1}. \tag{B.2}$$

For the special case of incompressibility one can use the representation $\mathbb{V}_{\mathsf{M}} = 2\mu_{\mathsf{M}}\mathbb{P}_2$ and $\mathbb{V}_{\mathsf{F}} = 2\mu_{\mathsf{F}}\mathbb{P}_2$ in Eq. (B.2) leading to

$$\mathbb{J}_{\mathsf{F}} = -\mathbb{E}^{\mathsf{A}}\mathbb{V}_{\mathsf{M}}^{-1}\left(\mathbb{V}_{\mathsf{F}}-\mathbb{V}_{\mathsf{M}}\right)\left(\mathbb{I}^{\mathsf{S}}+\mathbb{E}^{\mathsf{S}}\mathbb{V}_{\mathsf{M}}^{-1}\left(\mathbb{V}_{\mathsf{F}}-\mathbb{V}_{\mathsf{M}}\right)\right)^{-1}. \tag{B.3}$$

With the abbreviation $\delta\mathbb{V} = \mathbb{V}_{\mathsf{F}} - \mathbb{V}_{\mathsf{M}}$ and the expression for the polarization tensors $\mathbb{P}_0^{\mathsf{A,S}} = \mathbb{E}^{\mathsf{A,S}}\mathbb{V}_{\mathsf{M}}^{-1}$ given in, e.g., Walpole [101] (p. 196), the Jeffery tensor reads as follows

$$\mathbb{J}_{\mathsf{F}} = -\mathbb{P}_0^{\mathsf{A}}\delta\mathbb{V}\left(\mathbb{I}^{\mathsf{S}}+\mathbb{P}_0^{\mathsf{S}}\delta\mathbb{V}\right)^{-1} = -\mathbb{P}_0^{\mathsf{A}}\left(\delta\mathbb{V}^{-1}+\mathbb{P}_0^{\mathsf{S}}\right)^{-1}, \tag{B.4}$$

which can be further simplified based on the rigid fiber assumption (vanishing fluidity $\delta\mathbb{V}^{-1}$) [51,56] leading to the sought equivalence

$$\mathbb{J}_{\mathsf{F}} = -\mathbb{P}_0^{\mathsf{A}}\left(\mathbb{P}_0^{\mathsf{S}}\right)^{-1}. \tag{B.5}$$

Appendix C. Laplacian on the unit sphere

As a supplement to the derivation of the generalized fiber interaction term (37) involving the computation of the Laplacian on the unit sphere $\Delta_S(\boldsymbol{n}^{\otimes n})$, the special case of $n=2$ is considered in the following. Regarding the rules of calculus reference is made to, e.g., Sec. 2.3.4 of Sillem [89]. In index notation the Laplacian for $n=2$ reads

$$\begin{aligned}\left(\Delta_S(\boldsymbol{n}\otimes\boldsymbol{n})\right)_{ij} &= \frac{\partial^2 n_i n_j}{\partial n_k\partial n_k} = \frac{\partial}{\partial n_k}\left(\frac{\partial n_i n_j}{\partial n_k}\right) = \frac{\partial}{\partial n_k}\left(\frac{\partial n_i}{\partial n_k}n_j + n_i\frac{\partial n_j}{\partial n_k}\right)\\ &= \frac{\partial}{\partial n_k}\left(\left(\delta_{ik}-n_i n_k\right)n_j + n_i\left(\delta_{jk}-n_j n_k\right)\right)\\ &= \frac{\partial}{\partial n_k}\left(\delta_{ik}n_j + n_i\delta_{jk} - 2n_i n_j n_k\right).\end{aligned} \tag{C.1}$$

If one now applies the same procedure again and takes $\delta_{kk}=3$ and $n_k n_k = 1$ into account, this leads to

$$\begin{aligned}\left(\Delta_S(\boldsymbol{n}\otimes\boldsymbol{n})\right)_{ij} &= 2\left(\delta_{ij}-3n_i n_j\right),\\ \Delta_S(\boldsymbol{n}\otimes\boldsymbol{n}) &= 2\left(\boldsymbol{I}-3\boldsymbol{n}\otimes\boldsymbol{n}\right).\end{aligned} \tag{C.2}$$

If one now integrates this term, the well-known second-order fiber interaction term [18,19] follows by taking the properties of the orientation distribution function f and the definition of the second-order fiber orientation tensor $\boldsymbol{N}$ into account

$$\mathbb{D}_{\langle 2\rangle} = 2C_1\dot{\gamma}\int_S f(\boldsymbol{n})(\boldsymbol{I}-3\boldsymbol{n}\otimes\boldsymbol{n})\,\mathrm{d}S = 2C_1\dot{\gamma}(\boldsymbol{I}-3\boldsymbol{N}). \tag{C.3}$$

Appendix D. Polarization tensors

General definition. In contrast to the J, DD, and MT models discussed in Sections 2.3 to 2.5, the polarization tensors $\mathbb{P}_0^{\mathsf{A,S}}(\boldsymbol{n})$ must be computed explicitly for the PCW and EM models. In general, the polarization tensors for a spheroidal inclusion aligned with direction $\boldsymbol{n}$ are defined as follows [48,86]

$$\mathbb{P}_0^{\mathsf{A,S}} = \frac{1}{4\pi\det(\boldsymbol{Z}(\boldsymbol{n}))}\int_S \frac{\mathbb{H}^{\mathsf{A,S}}(\mathbb{V},\boldsymbol{p})}{\|\boldsymbol{Z}^{-1}(\boldsymbol{n})\boldsymbol{p}\|^3}\,\mathrm{d}S(\boldsymbol{p}), \tag{D.1}$$

with the definitions

$$\begin{aligned}&\mathbb{H}^{\mathsf{A,S}} = \mathbb{I}^{\mathsf{A,S}}\left(\boldsymbol{K}^{-1}\square(\boldsymbol{p}\otimes\boldsymbol{p})\right)\mathbb{I}^{\mathsf{S}},\\ &K_{ij} = V_{ikjl}p_k p_l,\\ &\boldsymbol{Z}_0 = \alpha^{-1}\boldsymbol{e}_1\otimes\boldsymbol{e}_1 + \boldsymbol{e}_2\otimes\boldsymbol{e}_2 + \boldsymbol{e}_3\otimes\boldsymbol{e}_3.\end{aligned} \tag{D.2}$$

The integration variable is represented by $\boldsymbol{p}$ to avoid confusion with the spheroidal inclusion direction $\boldsymbol{n}$. In general, the viscosity tensor of the matrix $\mathbb{V}$ can be arbitrarily anisotropic and $\boldsymbol{Z}_0$ stands for the reference shape tensor with $\boldsymbol{n}=\boldsymbol{e}_1$. For an arbitrary direction $\boldsymbol{n}$, the components $Z_{ij}(\boldsymbol{n})$ must be computed via $Z_{ij}(\boldsymbol{n}) = Q_{ik}(\boldsymbol{n})Z^0_{kl}Q^{\mathsf{T}}_{lj}(\boldsymbol{n})$. The computation of $Q_{ij}(\boldsymbol{n})$ is described in the following in order to make the manuscript self-contained. The angles $\theta\in[0,\pi]$ and $\varphi\in[0,2\pi)$ depend on the direction $\boldsymbol{n}$ as follows

$$\theta = \arccos(n_3), \qquad \varphi = \begin{cases}\arctan\left(\frac{n_2}{n_1}\right), & n_1>0\\ \mathrm{sgn}(n_2)\frac{\pi}{2}, & n_1=0\\ \arctan\left(\frac{n_2}{n_1}\right)+\pi, & n_1<0, n_2\geq 0\\ \arctan\left(\frac{n_2}{n_1}\right)-\pi, & n_1<0, n_2<0,\end{cases} \tag{D.3}$$

with which the components $Q_{ij}(\boldsymbol{n})$ are computed

$$Q_{ij} = \begin{pmatrix}\sin(\theta)\cos(\varphi) & \cos(\theta)\cos(\varphi) & -\sin(\varphi)\\ \sin(\theta)\sin(\varphi) & \cos(\theta)\sin(\varphi) & \cos(\varphi)\\ \cos(\theta) & -\sin(\theta) & 0\end{pmatrix}. \tag{D.4}$$

Efficient computation for the PCW model. For the special case of an isotropic and incompressible matrix fluid, the symmetric reference polarization tensor $\mathbb{P}_0^{\mathsf{S}}(\boldsymbol{e}_1)$ can be computed as follows [49] (in normalized Voigt or Mandel notation, see, e.g., Mandel [102] or Böhlke and

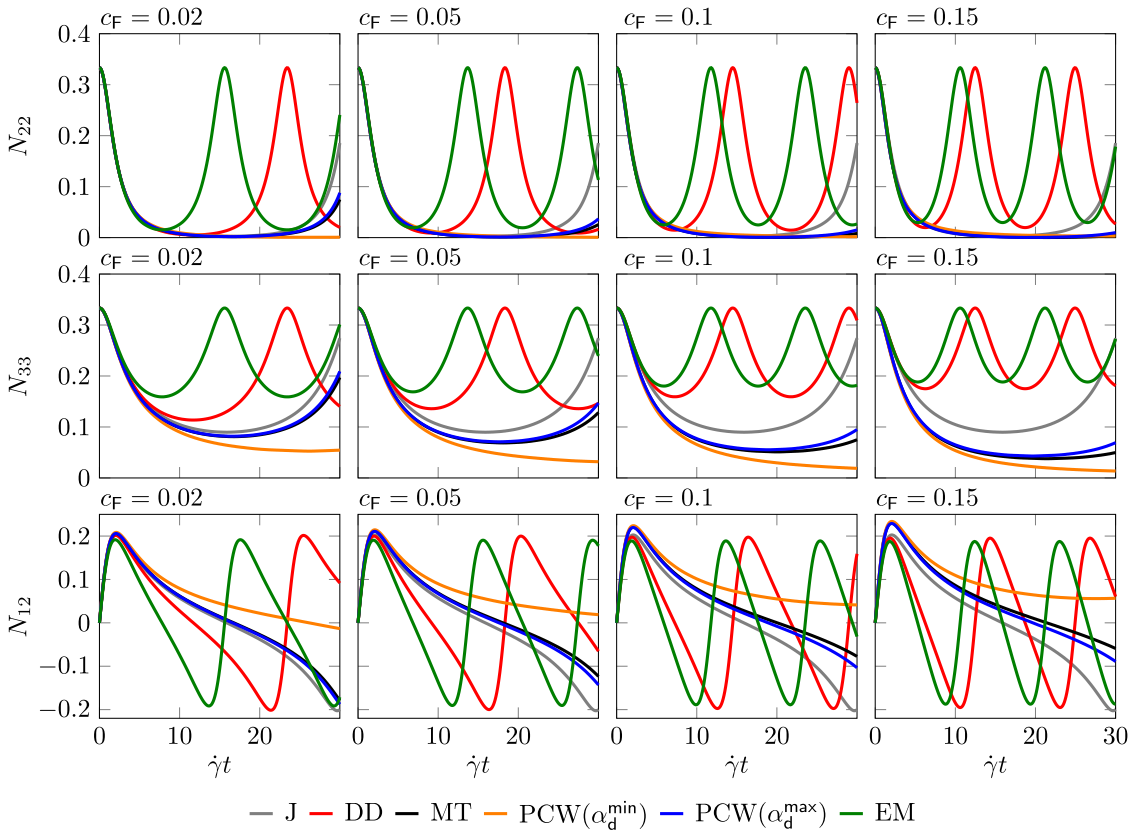

Fig. E.4. For the selected mean-field models DD, MT, PCW and EM, the evolution of the orientation tensor components N_{22}, N_{33} and N_{12} in a simple shear flow is plotted over the total shear $\dot{\gamma}t$. Each line refers to the respective orientation tensor component. The results of the Jeffery equation (J) are given for comparison. The different fiber volume fractions $c_F = 0.02, 0.05, 0.1$ and 0.15 refer to the respective column. The legend is valid for all subplots.

Brüggemann [103])

$$\mathbb{P}_0^S(\boldsymbol{e}_1)_{ijkl} = \begin{pmatrix} n & l & l & 0 & 0 & 0 \\ l & k+m & k-m & 0 & 0 & 0 \\ l & k-m & k+m & 0 & 0 & 0 \\ 0 & 0 & 0 & 2m & 0 & 0 \\ 0 & 0 & 0 & 0 & 2r & 0 \\ 0 & 0 & 0 & 0 & 0 & 2r \end{pmatrix}, \tag{D.5}$$

with the components simplified for incompressibility [56]

$$\begin{aligned} k &= \frac{h(\alpha) - 2\alpha^2 + 2\alpha^2 h(\alpha)}{8(1-\alpha^2)\mu_s}, \\ l &= \frac{2\alpha^2 - h(\alpha) - 2\alpha^2 h(\alpha)}{4(1-\alpha^2)\mu_s}, \\ n &= \frac{h(\alpha) - 2\alpha^2 + 2\alpha^2 h(\alpha)}{2(1-\alpha^2)\mu_s}, \\ m &= \frac{3h(\alpha) - 2\alpha^2}{16(1-\alpha^2)\mu_s}, \\ r &= \frac{2 - 3h(\alpha) + 2\alpha^2 - 3\alpha^2 h(\alpha)}{8(1-\alpha^2)\mu_s}, \\ h(\alpha) &= \frac{\alpha\left(\alpha\sqrt{\alpha^2-1} - \operatorname{arcosh}(\alpha)\right)}{(\alpha^2-1)^{3/2}}. \end{aligned} \tag{D.6}$$

Instead of integrating Eq. (D.1), one can simply compute $\mathbb{P}_0^S(\boldsymbol{e}_1)$ and use the transformation rule given in Kuzmin (p. 3047) [104] referring to the standard Voigt notation (see, e.g., Cowin [105]) leading to the sought rotated polarization tensor $\mathbb{P}_0^S(\boldsymbol{n})$. It should be noted that the rotation matrix Q_{ij} of Kuzmin [104] refers to Q_{ij}^T given in Eq. (D.4). Next, the Jeffery tensor $\mathbb{J}_F(\boldsymbol{n})$ referring to the direction $\boldsymbol{n}$ can be computed as given in Eq. (30). By using the shown equivalence (B.5), the sought rotated polarization tensor $\mathbb{P}_0^A(\boldsymbol{n})$ is computed via

$$\mathbb{P}_0^A(\boldsymbol{n}) = -\mathbb{J}_F(\boldsymbol{n})\mathbb{P}_0^S(\boldsymbol{n}). \tag{D.7}$$

To conclude, it should be noted that the described procedure refers to the assumption that both the inclusions (i) and the distribution (d) are modeled as spheroids with the aspect ratios α_i and α_d, respectively.

Appendix E. Additional results

Fig. E.4 shows the evolution of the orientation tensor components N_{22}, N_{33} and N_{12} for the considered mean-field models and fiber volume fractions as a supplement to Fig. 1 in Section 3. Fig. E.5 shows the orientation evolution of a single fiber on the unit sphere for different fiber volume fractions of the surrounding fiber suspension as a supplement to Fig. 2 in Section 3.

Appendix F. Supplementary material

Supplementary material related to this article can be found online at https://doi.org/10.1016/j.ijmecsci.2023.108771.

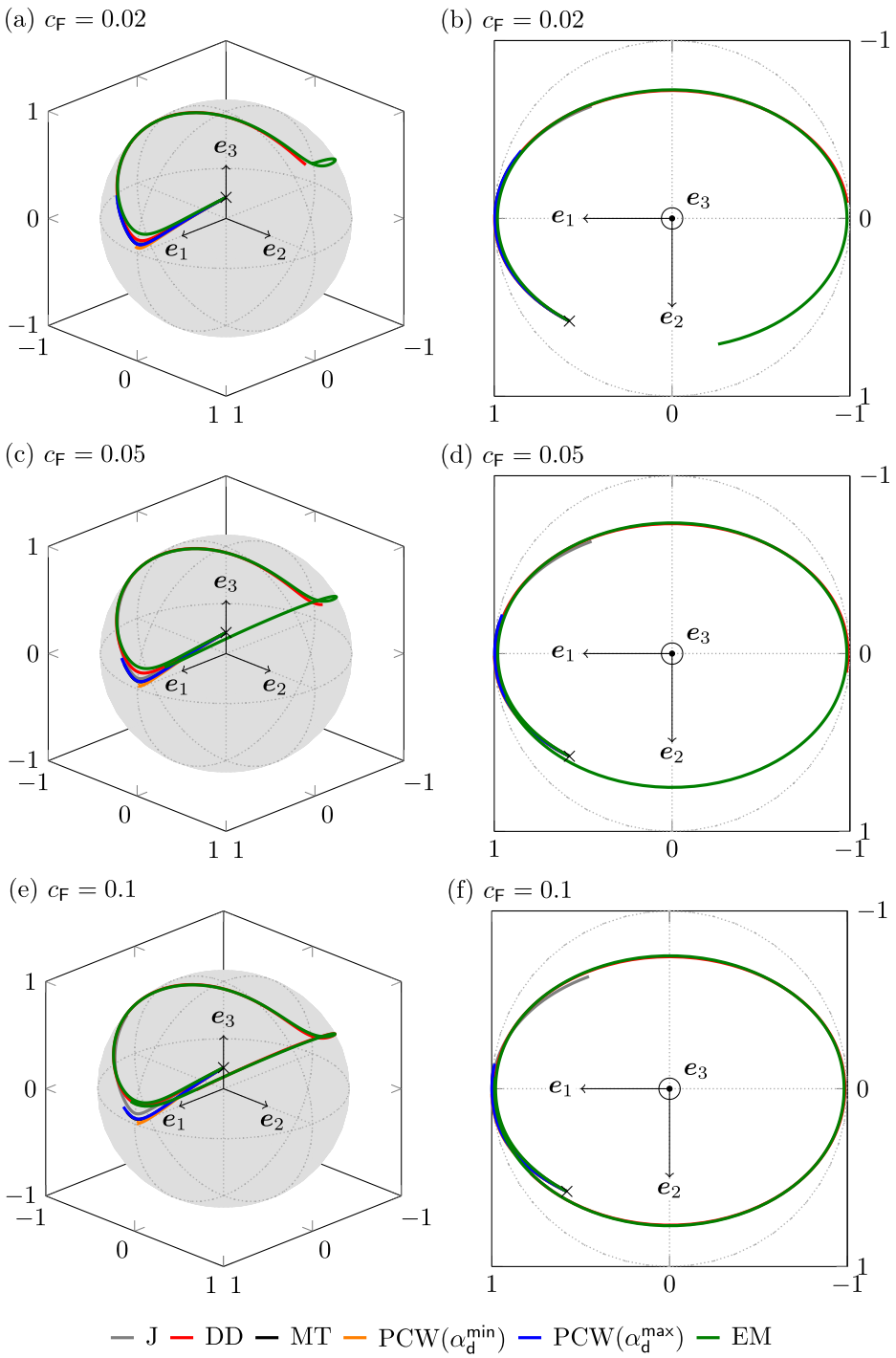

Fig. E.5. For the fiber volume fractions $c_F = 0.02$, 0.05 and 0.1 of the surrounding fiber suspension, the orientation behavior of a single fiber is shown for a simple shear flow with respect to the selected mean-field models DD, MT, PCW and EM. The Jeffery model (J) is considered as a reference. The initial fiber orientation is marked with ×. In (a), (c), (e), the orientation path of the single fiber is plotted on the unit sphere. The respective projection on the e_1–e_2-plane is shown in (b), (d), (f) for each fiber volume fraction. The legend is valid for all subplots.

References

[1] Tucker III CL. Fundamentals of fiber orientation: Description, measurement and prediction. 1st Edition. München: Carl Hanser Verlag; 2022.

[2] Böhlke T, Henning F, Hrymak A, Kärger L, Weidenmann K, Wood JT. Continuous-discontinuous fiber-reinforced polymers: An integrated engineering approach. 1st Edition. München: Carl Hanser Verlag; 2019.

[3] Görthofer J, Meyer N, Pallicity TD, Schöttl L, Trauth A, Schemmann M, et al. Virtual process chain of sheet molding compound: Development, validation and perspectives. Composites Part B: Eng 2019;169:133–47. http://dx.doi.org/10.1016/j.compositesb.2019.04.001.

[4] Meyer N, Gajek S, Görthofer J, Hrymak A, Kärger L, Henning F, et al. A probabilistic virtual process chain to quantify process-induced uncertainties in sheet molding compounds. Composites B 2023;249:110380. http://dx.doi.org/10.1016/j.compositesb.2022.110380.

[5] Jeffery GB. The motion of ellipsoidal particles immersed in a viscous fluid. Proc R Soc London Ser A 1922;102(715):161–79. http://dx.doi.org/10.1098/rspa.1922.0078.

[6] Junk M, Illner R. A new derivation of Jeffery's equation. J Math Fluid Mech 2007;9(4):455–88. http://dx.doi.org/10.1007/s00021-005-0208-0.

[7] Perez M, Scheuer A, Abisset-Chavanne E, Chinesta F, Keunings R. A multi-scale description of orientation in simple shear flows of confined rod suspensions.

J Non-Newton Fluid Mech 2016;233:61–74. http://dx.doi.org/10.1016/j.jnnfm.2016.01.011.
[8] Scheuer A, Abisset-Chavanne E, Chinesta F, Keunings R. Second-gradient modelling of orientation development and rheology of dilute confined suspensions. J Non-Newton Fluid Mech 2016;237:54–64. http://dx.doi.org/10.1016/j.jnnfm.2016.10.004.
[9] Einarsson J, Angilella J, Mehlig B. Orientational dynamics of weakly inertial axisymmetric particles in steady viscous flows. Physica D: Nonlinear Phenom 2014;278-279:79–85. http://dx.doi.org/10.1016/j.physd.2014.04.002.
[10] Einarsson J, Candelier F, Lundell F, Angilella JR, Mehlig B. Rotation of a spheroid in a simple shear at small Reynolds number. Phys Fluids 2015;27(6):063301. http://dx.doi.org/10.1063/1.4921543.
[11] Scheuer A, Grégoire G, Abisset-Chavanne E, Chinesta F, Keunings R. Modelling the effect of particle inertia on the orientation kinematics of fibres and spheroids immersed in a simple shear flow. Comput Math Appl 2020;79(3):539–54. http://dx.doi.org/10.1016/j.camwa.2018.12.039.
[12] Abtahi SA, Elfring GJ. Jeffery orbits in shear-thinning fluids. Phys Fluids 2019;31(10):103106. http://dx.doi.org/10.1063/1.5125468.
[13] Férec J, Bertevas E, Khoo BC, Ausias G, Phan-Thien N. Rigid fiber motion in slightly non-Newtonian viscoelastic fluids. Phys Fluids 2021;33(10):103320. http://dx.doi.org/10.1063/5.0064191.
[14] Borzacchiello D, Abisset-Chavanne E, Chinesta F, Keunings R. Orientation kinematics of short fibres in a second-order viscoelastic fluid. Rheol Acta 2016;55(5):397–409. http://dx.doi.org/10.1007/s00397-016-0929-4.
[15] Ishimoto K. Helicoidal particles and swimmers in a flow at low Reynolds number. J Fluid Mech 2020;892:A11. http://dx.doi.org/10.1017/jfm.2020.142.
[16] Ishimoto K. Jeffery orbits for an object with discrete rotational symmetry. Phys Fluids 2020;32(8):081904. http://dx.doi.org/10.1063/5.0015056.
[17] Kanatani K-I. Distribution of directional data and fabric tensors. Internat J Engrg Sci 1984;22(2):149–64. http://dx.doi.org/10.1016/0020-7225(84)90090-9.
[18] Advani SG, Tucker III CL. The use of tensors to describe and predict fiber orientation in short fiber composites. J Rheol 1987;31(8):751–84. http://dx.doi.org/10.1122/1.549945.
[19] Folgar F, Tucker III CL. Orientation behavior of fibers in concentrated suspensions. J Reinf Plast Compos 1984;3(2):98–119. http://dx.doi.org/10.1177/073168448400300201.
[20] Wang J, O'Gara JF, Tucker III CL. An objective model for slow orientation kinetics in concentrated fiber suspensions: Theory and rheological evidence. J Rheol 2008;52(5):1179–200. http://dx.doi.org/10.1122/1.2946437.
[21] Phelps JH, Tucker III CL. An anisotropic rotary diffusion model for fiber orientation in short- and long-fiber thermoplastics. J Non-Newton Fluid Mech 2009;156(3):165–76. http://dx.doi.org/10.1016/j.jnnfm.2008.08.002.
[22] Altan MC, Güceri SI, Pipes RB. Anisotropic channel flow of fiber suspensions. J Non-Newton Fluid Mech 1992;42(1):65–83. http://dx.doi.org/10.1016/0377-0257(92)80005-I.
[23] Tang L, Altan MC. Entry flow of fiber suspensions in a straight channel. J Non-Newton Fluid Mech 1995;56(2):183–216. http://dx.doi.org/10.1016/0377-0257(94)01280-U.
[24] Mezi D, Ausias G, Advani SG, Férec J. Fiber suspension in 2D nonhomogeneous flow: The effects of flow/fiber coupling for Newtonian and power-law suspending fluids. J Rheol 2019;63(3):405–18. http://dx.doi.org/10.1122/1.5081016.
[25] Wittemann F, Maertens R, Kärger L, Henning F. Injection molding simulation of short fiber reinforced thermosets with anisotropic and non-Newtonian flow behavior. Composites A 2019;124:105476. http://dx.doi.org/10.1016/j.compositesa.2019.105476.
[26] Karl T, Gatti D, Böhlke T, Frohnapfel B. Coupled simulation of flow-induced viscous and elastic anisotropy of short-fiber reinforced composites. Acta Mech 2021;232(6):2249–68. http://dx.doi.org/10.1007/s00707-020-02897-z.
[27] Karl T, Zartmann J, Dalpke S, Gatti D, Frohnapfel B, Böhlke T. Influence of flow–fiber coupling during mold-filling on the stress field in short-fiber reinforced composites. Comput Mech 2023;71(5):991–1013. http://dx.doi.org/10.1007/s00466-023-02277-z.
[28] Gilormini P, Chinesta F. Viscous drag and rod orientation kinematics in an orthotropic fluid. J Non-Newton Fluid Mech 2019;270:96–103. http://dx.doi.org/10.1016/j.jnnfm.2019.07.006.
[29] Mori T, Tanaka K. Average stress in matrix and average elastic energy of materials with misfitting inclusions. Acta Metall 1973;21(5):571–4. http://dx.doi.org/10.1016/0001-6160(73)90064-3.
[30] Benveniste Y. A new approach to the application of Mori–Tanaka's theory in composite materials. Mech Mater 1987;6(2):147–57. http://dx.doi.org/10.1016/0167-6636(87)90005-6.
[31] Chung DH, Kwon TH. Invariant-based optimal fitting closure approximation for the numerical prediction of flow-induced fiber orientation. J Rheol 2002;46(1):169–94. http://dx.doi.org/10.1122/1.1423312.
[32] Fletcher RC. Deformable, rigid, and inviscid elliptical inclusions in a homogeneous incompressible anisotropic viscous fluid. J Struct Geol 2009;31(4):382–7. http://dx.doi.org/10.1016/j.jsg.2009.01.006.
[33] Favaloro AJ. The rotation of rigid spheroids in a viscous fluid under mean-field effects. J Non-Newton Fluid Mech 2020;282:104324. http://dx.doi.org/10.1016/j.jnnfm.2020.104324.
[34] Reuss A. Berechnung der Fließgrenze von Mischkristallen auf Grund der Plastizitätsbedingung für Einkristalle. Z Angew Math Mech 1929;9(1):49–58. http://dx.doi.org/10.1002/zamm.19290090104.
[35] Férec J, Ausias G, Heuzey MC, Carreau PJ. Modeling fiber interactions in semiconcentrated fiber suspensions. J Rheol 2009;53(1):49–72. http://dx.doi.org/10.1122/1.3000732.
[36] Férec J, Abisset-Chavanne E, Ausias G, Chinesta F. On the use of interaction tensors to describe and predict rod interactions in rod suspensions. Rheol Acta 2014;53(5):445–56. http://dx.doi.org/10.1007/s00397-014-0767-1.
[37] Wetzel ED, Tucker III CL. Droplet deformation in dispersions with unequal viscosities and zero interfacial tension. J Fluid Mech 2001;426:199–228. http://dx.doi.org/10.1017/S0022112000002275.
[38] Wetzel ED. Modeling flow-induced microstructure of inhomogeneous liquid-liquid mixtures (Doctoral thesis), University of Illinois at Urbana-Champaign; 1999, http://hdl.handle.net/2142/83987.
[39] Eshelby JD. The determination of the elastic field of an ellipsoidal inclusion, and related problems. Proc R Soc London Ser A Math Phys Sci 1957;241(1226):376–96. http://dx.doi.org/10.1098/rspa.1957.0133.
[40] Eshelby JD. The elastic field outside an ellipsoidal inclusion. Proc R Soc London Ser A. Math Phys Sci 1959;252(1271):561–9. http://dx.doi.org/10.1098/rspa.1959.0173.
[41] Bilby B, Eshelby J, Kundu A. The change of shape of a viscous ellipsoidal region embedded in a slowly deforming matrix having a different viscosity. Tectonophysics 1975;28(4):265–74. http://dx.doi.org/10.1016/0040-1951(75)90041-4.
[42] Howard I, Brierley P. On the finite deformation of an inhomogeneity in a viscous liquid. Internat J Engrg Sci 1976;14(12):1151–9. http://dx.doi.org/10.1016/0020-7225(76)90080-X.
[43] Bilby BA, Kolbuszewski ML, Eshelby JD. The finite deformation of an inhomogeneity in two-dimensional slow viscous incompressible flow. Proc R Soc Lond Ser A Math Phys Eng Sci 1977;355(1682):335–53. http://dx.doi.org/10.1098/rspa.1977.0101.
[44] Tucker III CL, Liang E. Stiffness predictions for unidirectional short-fiber composites: Review and evaluation. Compos Sci Technol 1999;59(5):655–71. http://dx.doi.org/10.1016/S0266-3538(98)00120-1.
[45] Ponte Castañeda P. Anisotropic Oldroyd-type models for non-colloidal suspensions of viscoelastic particles in Newtonian and yield-stress fluids via homogenization. J Non-Newton Fluid Mech 2021;295:104625. http://dx.doi.org/10.1016/j.jnnfm.2021.104625.
[46] Avazmohammadi R, Ponte Castañeda P. The rheology of non-dilute dispersions of highly deformable viscoelastic particles in Newtonian fluids. J Fluid Mech 2015;763:386–432. http://dx.doi.org/10.1017/jfm.2014.687.
[47] Hashin Z, Shtrikman S. A variational approach to the theory of the elastic behaviour of multiphase materials. J Mech Phys Solids 1963;11(2):127–40. http://dx.doi.org/10.1016/0022-5096(63)90060-7.
[48] Willis J. Bounds and self-consistent estimates for the overall properties of anisotropic composites. J Mech Phys Solids 1977;25(3):185–202. http://dx.doi.org/10.1016/0022-5096(77)90022-9.
[49] Ponte Castañeda P, Willis J. The effect of spatial distribution on the effective behavior of composite materials and cracked media. J Mech Phys Solids 1995;43(12):1919–51. http://dx.doi.org/10.1016/0022-5096(95)00058-Q.
[50] Schneider M. On the effective viscosity of a periodic suspension – analysis of primal and dual formulations for Newtonian and non-Newtonian solvents. Math Methods Appl Sci 2016;39(12):3309–27. http://dx.doi.org/10.1002/mma.3775.
[51] Bertóti R, Wicht D, Hrymak A, Schneider M, Böhlke T. A computational investigation of the effective viscosity of short-fiber reinforced thermoplastics by an FFT-based method. Eur J Mech B/Fluids 2021;90:99–113. http://dx.doi.org/10.1016/j.euromechflu.2021.08.004.
[52] Sterr B, Wicht D, Hrymak A, Schneider M, Böhlke T. Homogenizing the viscosity of shear-thinning fiber suspensions with an FFT-based computational method. J Non-Newton Fluid Mech 2023;321:105101. http://dx.doi.org/10.1016/j.jnnfm.2023.105101.
[53] Bertóti R, Böhlke T. Flow-induced anisotropic viscosity in short FRPs. Mech Adv Mater Modern Process 2017;3(1). http://dx.doi.org/10.1186/s40759-016-0016-7.
[54] Dinh SM, Armstrong RC. A rheological equation of state for semi-concentrated fiber suspensions. J Rheol 1984;28(3):207–27. http://dx.doi.org/10.1122/1.549748.
[55] Traxl R, Pichler C, Lackner R. Micromechanics-based assessment of the effective viscosity of suspensions of generalized-Newtonian fluids embedding noncolloidal angular/spheroidal pores and particles. J Rheol 2020;64(4):899–913. http://dx.doi.org/10.1122/1.5139932.
[56] Karl T, Böhlke T. Unified mean-field modeling of viscous short-fiber suspensions and solid short-fiber reinforced composites. Arch Appl Mech 2022;92(12):3695–727. http://dx.doi.org/10.1007/s00419-022-02257-4.
[57] Hill R. Elastic properties of reinforced solids: Some theoretical principles. J Mech Phys Solids 1963;11(5):357–72. http://dx.doi.org/10.1016/0022-5096(63)90036-X.
[58] Mandel J. Generalization dans R9 de la regle du potential plastique pour un element polycrystallin. C R l'Acad Sci 1980;290(22):481–4.

[59] Adams B, Field D. A statistical theory of creep in polycrystalline materials. Acta Metall Mater 1991;39(10):2405–17. http://dx.doi.org/10.1016/0956-7151(91)90021-R.

[60] Kammer C, Blackwell B, Arratia PE, Ponte Castañeda P. A homogenization model for the rheology and local field statistics of suspensions of particles in yield stress fluids. J Rheol 2022;66(3):535–49. http://dx.doi.org/10.1122/8.0000337.

[61] Hill R. A self-consistent mechanics of composite materials. J Mech Phys Solids 1965;13(4):213–22. http://dx.doi.org/10.1016/0022-5096(65)90010-4.

[62] Budiansky B. On the elastic moduli of some heterogeneous materials. J Mech Phys Solids 1965;13(4):223–7. http://dx.doi.org/10.1016/0022-5096(65)90011-6.

[63] Kammer C, Ponte Castañeda P. Variational estimates for the effective properties and field statistics of composites with variable particle interaction strengths. J Mech Phys Solids 2022;167:104996. http://dx.doi.org/10.1016/j.jmps.2022.104996.

[64] Hill DA. Evolution equations for arbitrary moments of the orientation distribution of rigid-rod molecules. J Rheol 1999;43(6):1635–41. http://dx.doi.org/10.1122/1.551064.

[65] Böhlke T. Texture simulation based on tensorial Fourier coefficients. Comput Struct 2006;84(17):1086–94. http://dx.doi.org/10.1016/j.compstruc.2006.01.006.

[66] Papenfuss C. Mesoscopic continuum theory for liquid crystals. Atti Accad Peloritana Pericolanti - Classe Sci Fis, Mat Nat 2019;97(S1):A21. http://dx.doi.org/10.1478/AAPP.97S1A21.

[67] Moakher M, Basser PJ. Fiber orientation distribution functions and orientation tensors for different material symmetries. In: Hotz I, Schultz T, editors. Visualization and processing of higher order descriptors for multi-valued data. Cham: Springer International Publishing; 2015, p. 37–71. http://dx.doi.org/10.1007/978-3-319-15090-1_3.

[68] Böhlke T, Jöchen K, Piat R, Langhoff T-A, Tsukrov I, Reznik B. Elastic properties of pyrolytic carbon with axisymmetric textures. Tech Mech 2010;30(4):343–53, https://journals.ub.ovgu.de/index.php/techmech/article/view/803.

[69] Müller V, Böhlke T. Prediction of effective elastic properties of fiber reinforced composites using fiber orientation tensors. Compos Sci Technol 2016;130:36–45. http://dx.doi.org/10.1016/j.compscitech.2016.04.009.

[70] Bauer JK, Böhlke T. Variety of fiber orientation tensors. Math Mech Solids 2022;27(7):1185–211. http://dx.doi.org/10.1177/10812865211057602.

[71] Tyler DE. Statistical analysis for the angular central Gaussian distribution on the sphere. Biometrika 1987;74(3):579–89. http://dx.doi.org/10.2307/2336697.

[72] Montgomery-Smith S, He W, Jack DA, Smith DE. Exact tensor closures for the three-dimensional Jeffery's equation. J Fluid Mech 2011;680:321–35. http://dx.doi.org/10.1017/jfm.2011.165.

[73] Bingham C. An antipodally symmetric distribution on the sphere. Ann Statist 1974;2(6):1201–25. http://dx.doi.org/10.1214/aos/1176342874.

[74] Jaynes ET. Information theory and statistical mechanics. Phys Rev 1957;106(4):620–30. http://dx.doi.org/10.1103/PhysRev.106.620.

[75] Chaubal CV, Leal LG. A closure approximation for liquid-crystalline polymer models based on parametric density estimation. J Rheol 1998;42(1):177–201. http://dx.doi.org/10.1122/1.550887.

[76] van Gurp M. Letter to the editor: On the use of spherical tensors and the maximum entropy method to obtain closure for anisotropic liquids. J Rheol 1998;42(5):1269–71. http://dx.doi.org/10.1122/1.550921.

[77] Nabergoj M, Urevc J, Halilovič M. Function-based reconstruction of the fiber orientation distribution function of short-fiber-reinforced polymers. J Rheol 2022;66(1):147–60. http://dx.doi.org/10.1122/8.0000358.

[78] Tucker III CL. Planar fiber orientation: Jeffery, non-orthotropic closures, and reconstructing distribution functions. J Non-Newton Fluid Mech 2022;310:104939. http://dx.doi.org/10.1016/j.jnnfm.2022.104939.

[79] Lipinski P, Berveiller M. Elastoplasticity of micro-inhomogeneous metals at large strains. Int J Plast 1989;5(2):149–72. http://dx.doi.org/10.1016/0749-6419(89)90027-2.

[80] Lebensohn R, Tomé C. A self-consistent anisotropic approach for the simulation of plastic deformation and texture development of polycrystals: Application to zirconium alloys. Acta Metall Mater 1993;41(9):2611–24. http://dx.doi.org/10.1016/0956-7151(93)90130-K.

[81] Torquato S. Random heterogeneous materials: Microstructure and macroscopic properties. In: Interdisciplinary Applied Mathematics, Vol. 16. New York: Springer; 2002.

[82] Hashin Z, Shtrikman S. On some variational principles in anisotropic and nonhomogeneous elasticity. J Mech Phys Solids 1962;10(4):335–42. http://dx.doi.org/10.1016/0022-5096(62)90004-2.

[83] Hashin Z, Shtrikman S. A variational approach to the theory of the elastic behaviour of polycrystals. J Mech Phys Solids 1962;10(4):343–52. http://dx.doi.org/10.1016/0022-5096(62)90005-4.

[84] Walpole L. On bounds for the overall elastic moduli of inhomogeneous systems–I. J Mech Phys Solids 1966;14(3):151–62. http://dx.doi.org/10.1016/0022-5096(66)90035-4.

[85] Walpole L. On bounds for the overall elastic moduli of inhomogeneous systems–II. J Mech Phys Solids 1966;14(5):289–301. http://dx.doi.org/10.1016/0022-5096(66)90025-1.

[86] Willis J. Variational and related methods for the overall properties of composites. Adv Appl Mech 1981;21:1–78. http://dx.doi.org/10.1016/S0065-2156(08)70330-2.

[87] Lohmann C. Efficient algorithms for constraining orientation tensors in Galerkin methods for the Fokker–Planck equation. Comput Math Appl 2016;71(5):1059–73. http://dx.doi.org/10.1016/j.camwa.2016.01.012.

[88] Fokker AD. Die mittlere Energie rotierender elektrischer Dipole im Strahlungsfeld. Ann Phys 1914;348(5):810–20. http://dx.doi.org/10.1002/andp.19143480507.

[89] Sillem A. Fundamental theory and implementation of the Wang-O'Gara-Tucker model for the modeling of fiber orientation in fiber filled injection molded thermoplastics (Master thesis), Faculty of Mechanical, Maritime and Materials Engineering. Delft University of Technology; 2010, http://resolver.tudelft.nl/uuid:d9406a21-b7fe-49fe-a4b4-fe2082dd6e87.

[90] Latz A, Strautins U, Niedziela D. Comparative numerical study of two concentrated fiber suspension models. J Non-Newton Fluid Mech 2010;165(13):764–81. http://dx.doi.org/10.1016/j.jnnfm.2010.04.001.

[91] Thevenin P, Perreux D. The use of homogenization methods for estimating anisotropic viscosities of composite melts. Compos Sci Technol 1996;56(5):595–603. http://dx.doi.org/10.1016/0266-3538(96)00046-2.

[92] Bertóti R. Modeling the flow-induced anisotropic effective viscosity of fiber suspensions by mean-field and full-field homogenization (Doctoral thesis), Schriftenreihe Kontinuumsmechanik im Maschinenbau Band 19. Karlsruher Institut für Technologie (KIT); 2021, http://dx.doi.org/10.5445/IR/1000131222.

[93] Du D, Zheng Q-S. A further exploration of the interaction direct derivative (IDD) estimate for the effective properties of multiphase composites taking into account inclusion distribution. Acta Mech 2002;157(1):61–80. http://dx.doi.org/10.1007/BF01182155.

[94] Kanaun SK, Levin VM. Self-consistent methods for composites, 1: Static problems of solid mechanics and its applications, Vol. 148. Dordrecht: Springer; 2008.

[95] Lebedev V, Laikov D. A quadrature formula for the sphere of the 131st algebraic order of accuracy. Dokl Math 1999;59(3):477–81.

[96] Parrish R. getLebedevSphere. matlab® central file exchange. 2021, Retrieved July 6, 2021, https://www.mathworks.com/matlabcentral/fileexchange/27097-getlebedevsphere.

[97] Schürmann H. Konstruieren mit Faser-Kunststoff-Verbunden. 2nd Edition. Berlin, Heidelberg: Springer; 2007.

[98] Tucker III CL. Flow regimes for fiber suspensions in narrow gaps. J Non-Newton Fluid Mech 1991;39(3):239–68. http://dx.doi.org/10.1016/0377-0257(91)80017-E.

[99] Karl T, Schneider M, Böhlke T. On fully symmetric implicit closure approximations for fiber orientation tensors. J Non-Newton Fluid Mech 2023;318:105049. http://dx.doi.org/10.1016/j.jnnfm.2023.105049.

[100] Kumar A, Dawson PR. The simulation of texture evolution with finite elements over orientation space I. Development. Comput Methods Appl Mech Engrg 1996;130(3):227–46. http://dx.doi.org/10.1016/0045-7825(95)00904-3.

[101] Walpole L. Elastic behavior of composite materials: Theoretical foundations. Adv Appl Mech 1981;21:169–242. http://dx.doi.org/10.1016/S0065-2156(08)70332-6.

[102] Mandel J. Generalisation de la theorie de plasticite de W. T. Koiter. Int J Solids Struct 1965;1(3):273–95. http://dx.doi.org/10.1016/0020-7683(65)90034-X.

[103] Böhlke T, Brüggemann C. Graphical representation of the generalized Hooke's law. Tech Mech 2001;21(2):145–58, https://journals.ub.uni-magdeburg.de/ubjournals/index.php/techmech/article/view/1045.

[104] Kuzmin D. Planar and orthotropic closures for orientation tensors in fiber suspension flow models. SIAM J Appl Math 2018;78(6):3040–59. http://dx.doi.org/10.1137/18M1175665.

[105] Cowin SC. Properties of the anisotropic elasticity tensor. Quart J Mech Appl Math 1989;42(2):249–66. http://dx.doi.org/10.1093/qjmam/42.2.249.